European Journal of Medicinal Chemistry 305 (2026) 118486

Contents lists available at ScienceDirect

European Journal of Medicinal Chemistry

journal homepage: www.elsevier.com/locate/ejmech

Research paper

Targeting neuroinflammation by activation of the sigma-1 receptor (S1R) and inhibition of butyrylcholinesterase (*h*BChE) leads to highly potent anti-amnesic compounds in an Alzheimer's disease mouse model

Kora Reichau [a], Lucie Crouzier [b], Tina Gehrig [a], Alix Flake [a], Eva Schaller [a], Johann Meunier [b], Christelle Bertrand-Gaday [c], Arnaud Chatonnet [c], Liga Zvejniece [d], Christoph Sotriffer [a], Tangui Maurice [b,*], Michael Decker [a,**]

[a] *Pharmazeutische und Medizinische Chemie, Institut für Pharmazie und Lebensmittelchemie, Julius-Maximilians-Universität Würzburg (JMU), Am Hubland, Würzburg, 97074, Germany*
[b] *MMDN, University of Montpellier, EPHE, INSERM, Montpellier, France*
[c] *DMEM, University of Montpellier, INRAE, Montpellier, France*
[d] *Laboratory of Pharmaceutical Pharmacology, Latvian Institute of Organic Synthesis, Riga, LV-1006, Latvia*

ARTICLE INFO

Keywords:
Butyrylcholinesterase
Sigma-1 receptor
Multi-target directed ligands
Alzheimer's disease
Neuroprotection

ABSTRACT

Alzheimer's disease (AD) is a neurodegenerative disorder for which no effective preventative or curative treatment has yet been identified. Due to the multifactorial nature and complex pathophysiology of the disease, we developed a multi-target ligand that both inhibits human butyrylcholinesterase (*h*BChE), a key enzyme linked to β-amyloid plaque formation, and activates the sigma-1 receptor (S1R), which modulates neuroinflammatory and protective pathways. To this end, a series of isoindolines were designed and synthesized, and their biological activities were evaluated. The most promising compound, **7c**, exhibited significant dual activity, achieving nanomolar IC_{50} values against *h*BChE and potent S1R activation. Subsequent *in vivo* studies in an $A\beta_{25\text{-}35}$ mouse model revealed a remarkable improvement in cognitive deficits in both short- and long-term memory at an effective dose of 0.01 mg/kg in WT Swiss-OF1 mice. This dose is 10-fold lower compared to single-target compounds **7a** and **7b** of this isoindoline series. The lack of neuroprotective effects in BChE knock-out (KO) mice confirmed the involvement of BChE inhibition in the pharmacological effects of compound **7c** in WT mice. Further combinatorial studies employing a two-drug combination demonstrated synergy in the neuroprotective effect of addressing the two targets.

1. Introduction

In 1907, Alois Alzheimer first characterized the neuropsychological and neuropathological changes of dementia observed in one of his patients [1]. Three years later, his mentor Emil Kraepelin first described this pathology as Alzheimer's disease (AD) in his "Handbuch der Psychiatrie". In the 1980s, our modern understanding of the disease and its neurological pathology started to accelerate [2]. Today, AD is considered a multifactorial neurodegenerative disease influenced by both genetic and environmental factors. Nevertheless, the exact mechanisms of AD pathology are still not fully understood, but at the same time crucial for the development of effective treatment strategies [3]. These treatments are urgently needed, as an ageing population leads to an increasing number of patients affected by dementia, the most common form of which is AD [4]. Currently, more than 57 million patients worldwide are suffering from AD and other dementias, with numbers expected to increase to 130 million until 2050 [5,6].

AD toxicity is characterized by various molecular and pathophysiological hallmarks. First, amyloid-β (Aβ) species are generated from improper cleavage of the amyloid precursor protein by secretases, resulting in the formation of reactive monomers that can aggregate into neurotoxic Aβ oligomers and fibrils [7]. Those fibrils aggregate into plaques leading to recruitment of microglia, which can clear Aβ via scavenger receptors but also express proinflammatory cytokines,

* Corresponding author.
** Corresponding author.
E-mail address: michael.decker@uni-wuerzburg.de (M. Decker).

https://doi.org/10.1016/j.ejmech.2025.118486
Received 21 October 2025; Received in revised form 9 December 2025; Accepted 10 December 2025
Available online 13 December 2025

neurotoxic reactive oxygen (ROS) and nitrogen species. Persistent Aβ production thereby causes a pathological inflammatory state. Additionally, those proinflammatory microglia also contribute to increased tau phosphorylation, another pathological hallmark of AD [8,9]. Hyperphosphorylated tau proteins lead to collapse of microtubules and aggregation into neurofibrillary tangles (NFTs) in neurons [10]. During the past years, research on the neuroinflammatory state of brains affected by AD provided evidence that systemic inflammation itself acts as main driver in AD progression [11,12]. Even though extensive research on the formation mechanisms of these processes and approaches targeting them were conducted, there is no effective disease-modifying treatment yet [13]. Due to this and AD's multifactorial nature, multi-target directed ligands aiming at efficiently alleviating neurotoxicity simultaneously, with the possibility of providing an over-additive therapeutic effect, are expected to represent promising treatment strategies [14–16].

An effective target, associated with both Aβ and NFTs is the enzyme butyrylcholinesterase (BChE) [17,18]. Darvesh *et al.* demonstrated association of BChE with fibrillar Aβ. Their knock-out of BChE expression in a transgenic AD mouse (BChE knock-out (KO) x 5XFAD) led to a significant reduction of Aβ aggregation, which supported the assumption of BChE involvement in Aβ formation [19]. Moreover, BChE is known to catalyze the hydrolysis of different choline and non-choline esters [20]. Its function to cleave the neurotransmitter acetylcholine (ACh) is also relevant in AD. In healthy brain, ACh is cleaved by acetylcholinesterase (AChE). However, during AD a significant loss of 55–67 % of AChE occurs while levels of BChE rise up to 120 % [21]. The ability of BChE to take over AChE's functions was shown in AChE KO mice, where BChE compensates the lack of AChE and maintained normal cholinergic pathways without overexpression [22,23]. Considering the increased expression of BChE in AD, its ability of ACh hydrolysis promotes the pathological loss of cholinergic neurons in the basal forebrain during AD [24]. Therefore, BChE seems to be the more prominent ChE to target in advanced AD and its proved connection to other key hallmarks of AD makes it a promising molecular target [25]. In the past years, several types of *h*BChE inhibitors for the treatment of AD have been investigated. Among them, diverse heterocyclic compounds are described like compounds **1**–**2** and tacrine derivatives like **3** (Fig. 1a). A prominent class of *h*BChE inhibitors is represented by carbamates (Fig. 1b), which predominantly act in a "pseudo-irreversible" inhibition mode, which means that the carbamate unit is transferred to the active site serine under the release of the carbamates' corresponding phenols, which can also possess biological activity. Subsequent slow hydrolysis off the serine reconstitutes enzyme activity [17]. In previous studies we could show neuroprotective effects of such carbamate-based *h*BChE inhibitors like **UW-MD-95** (Fig. 1b) [26–29]. In cellular models applying murine hippocampal neuronal (HT22) cells, **UW-MD-95** showed protective effects against glutamate-induced toxicity. Subsequent investigations in mouse models demonstrated neuroprotection in a 0.3–3 mg/kg dose range against $A\beta_{25\text{-}35}$-induced memory deficits [26]. Further *in vivo* studies showed that compound **UW-MD-95** also attenuated $A\beta_{25\text{-}35}$-induced neuroinflammation, oxidative stress and apoptosis and blocked $A\beta_{1\text{-}42}$ generation, suggesting a putative disease-modifying effect [28].

A second auspicious target with neuroprotective action in AD is the sigma-1 receptor (S1R) [34,35]. The S1R is in fact an intracellular chaperone protein, expressed in the endoplasmic reticulum (ER) membrane and particularly concentrated in mitochondria-associated ER membranes [36], where it interacts with numerous client proteins including the binding immunoglobulin protein (BiP) or the inositol-1,4,5 triphosphate receptor (IP_3R). Upon activation by ER, calcium depletion or ligand binding, S1R dissociates [36,37]. The chaperone then translocates and modulates various types of signaling pathways [37]. For example, S1R chaperones IP_3R and thereby regulates calcium homeostasis in mitochondria, supporting mitochondrial bioenergetics and cell survival [36]. S1R also modulates cytosolic calcium via ER–cytosol signaling, which affects calcium homeostasis with extracellular calcium through store-operated calcium entry [38,39]. Related to its calcium regulating functions, S1R activation represents an endogenous cytoprotective system against Aβ toxicity in AD, where membrane depolarization occurs by formation of calcium ion permeable pores [40]. S1R also regulates signaling pathways through interactions with various neurotransmitter systems including cholinergic and glutamatergic receptors. Glutamatergic modulation promotes neurogenesis mainly through brain-derived neurotrophic factor (BDNF), which supports neural plasticity and resilience in neurodegenerative conditions. Activation of S1R enhances BDNF secretion and TrkB signaling, fostering neuroprotection and synaptic plasticity, thereby contributing to improved cognition and neuronal survival [37,39,41]. Moreover, S1R regulates proper tau phosphorylation and axon extension by interaction with myristic acid during neuronal development. However, the details of S1R-tau interaction in AD still need to be studied [42].

Besides, S1R possesses a set of anti-inflammatory functions in the brain linked to AD. Studies showed that S1R activation by respective agonists (or activators) reduces oxidative stress by modulation of antioxidant response through upregulation of protective proteins resulting

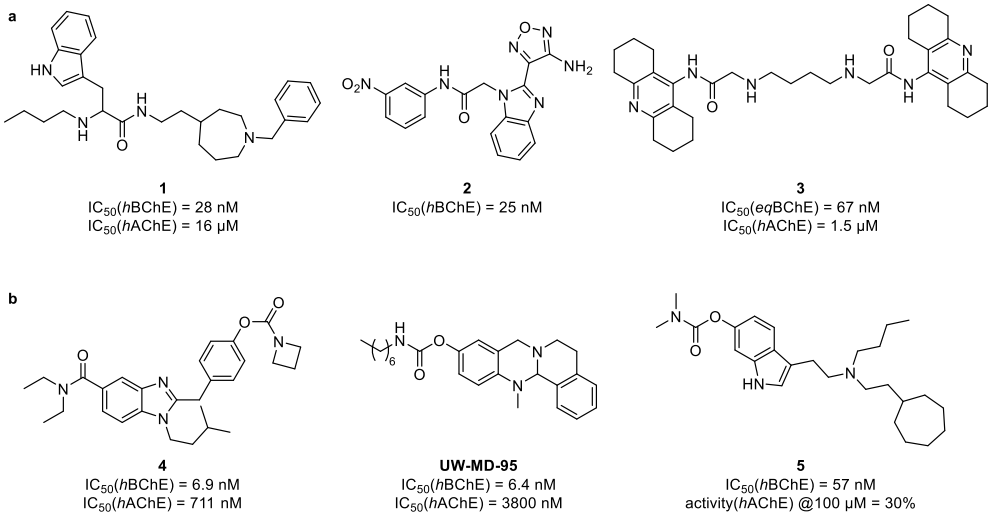

Fig. 1. Representative *h*BChE inhibitors. (**a**) Heterocyclic and tacrine derived inhibitors **1**-**3** [30–32]. (**b**) Carbamate inhibitors **4**, **UW-MD-95** and compound **5** [26–28,33].

in attenuation of ROS [43,44]. S1R can also block certain receptors on the microglia surface, which prevents cation influx and thereby activation and migration of proinflammatory microglia [45]. The neuroprotective potential of S1R agonists was demonstrated in cultures of rat cortical neurons, where ligand activation of S1R could prevent the toxic effects of Aβ proteins including the $A\beta_{25\text{-}35}$ fragment [46,47]. *In vivo* studies using mice with $A\beta_{25\text{-}35}$-induced learning impairments showed improved learning and memory deficits by treatment with S1R agonists like (+)-pentazocine, **PRE-084** and cutamesine (**SA4503**) (Fig. 2). These effects were blocked by known S1R antagonists [48]. The high potential of targeting S1R is also underlined by a positron emission tomography study of AD patients using the labelled S1R ligand [^{11}C]**SA4503** showing a significant loss of S1R in AD brain, which could be compensated by sustained S1R activation [49].

In this work, we aimed to develop "small molecule" hybrid compounds targeting both, *h*BChE and S1R, as extracellular and intracellular targets, respectively, with key involvement in neuroinflammation and therefore opening the way to neuroprotection by respective inhibitors and agonists. We rationally designed and synthesized novel hybrid molecules and evaluated these ligands *in vitro* and *in vivo* as AD experimental therapeutics in an $A\beta_{25\text{-}35}$ mouse model. Starting point for the hybrids' design were our described *h*BChE inhibitors (Fig. 3b), which show pronounced activity through (pseudo-)irreversible transfer of the carbamate moiety to the active-site serine of *h*BChE [27,53]. The benzimidazole scaffold itself, however, does not inhibit *h*BChE, but instead promotes selectivity over *h*AChE [27]. This makes the benzimidazole an exchangeable motif, enabling introduction of S1R pharmacophores. The features for S1R affinity are described by Glennon's model [54]. The principal pharmacophore is a basic amine that promotes binding through charge-charge interactions with a glutamate residue. This amine is surrounded by two hydrophobic pockets in a specified distance (Fig. 3a) [54,55]. A motif that aligns with these criteria and shares structural similarities with the original benzimidazole is isoindoline. Various substituted isoindolines, such as ligand **6** (Fig. 3b), were previously investigated by Linkens *et al.* and demonstrated high affinity for S1R [56]. This supports our hypothesis that employing an isoindoline to emulate the benzimidazole in compound **4** could elegantly yield a merged structure with dual activity. Furthermore, docking studies conducted by Linkens *et al.* indicated that the morpholine ring is situated in the larger primary hydrophobic pocket in proximity to a tyrosine residue [56]. To enhance binding, our objective was to incorporate aryl residues, which could potentially promote hydrophobic interactions in the primary pocket, as opposed to utilizing the hydrophilic morpholine present in the parent structure **6** (Fig. 3b). To this end, we introduced a simple phenyl and a more flexible benzyl residue in 5-position. At the carbamate site, two different residues were employed: Initially, a heptyl chain was utilized, which was demonstrated to greatly enhance selectivity over *h*AChE and could offset a potential deficiency in selectivity through the exchange of the benzimidazole scaffold [27,57–59]. The second carbamate residue, an azetidine, constituted the most-effective compounds in our previous work [27], resulting in more "druglike" low molecular weight and lipophilicity compared to heptyl carbamates.

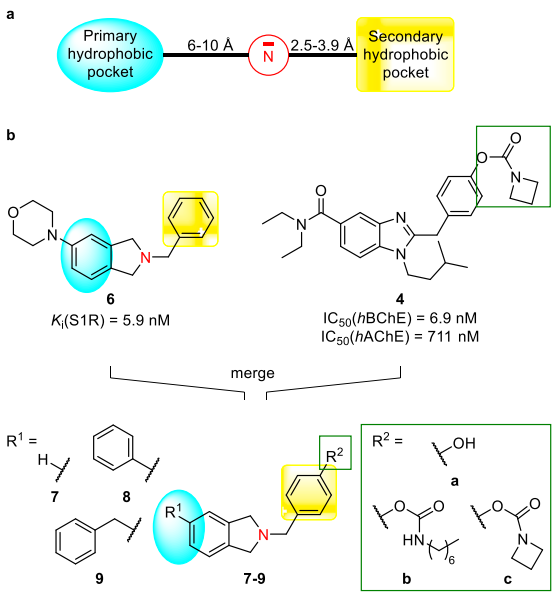

Fig. 3. (**a**) Glennon's model for S1R ligands [54]. (**b**) Top left: representative isoindoline S1R ligand **6** discovered by Linkens *et al.* [56] color-coded according to Glennon's model. Top right: representative *h*BChE inhibitor **4** discovered by Spatz *et al.* with carbamate unit transferred to *h*BChE highlighted by a green box [27]. Bottom: Merged ligand by combining both structures above with indication of the respective pharmacophores.

2. Results and discussion

2.1. Chemistry

Synthesis started with isoindoline **10** which was substituted with 1-(chloromethyl)-4-methoxybenzene to give the respective *N*-benzylisoindoline **13** in high yields (Scheme 1). For derivatives **14** and **15** with aromatic substituents in 5-position, 5-bromoisoindoline **11** was used instead and the formed product **12** was obtained in 51 % yield. Bromide **12** was then coupled in a Suzuki reaction with the according aryl bromides to give 5-phenylisoindoline **14** and 5-benzylisoindoline **15**, respectively, in good yields. Next, methyl ethers **13–15** were cleaved using boron tribromide to yield phenols **7a**, **8a**, and **9a**, respectively, in good yields. Finally, corresponding carbamates were formed from these

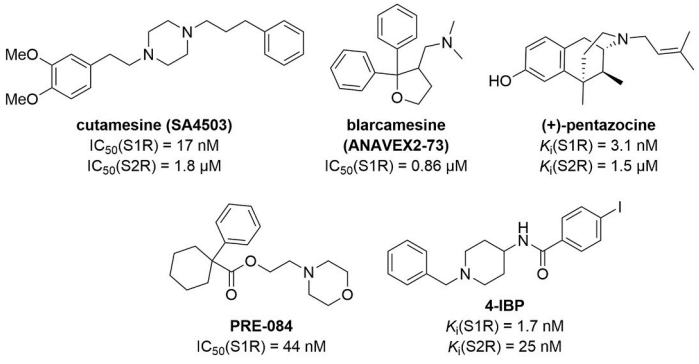

Fig. 2. Selected S1R ligands [50–52].

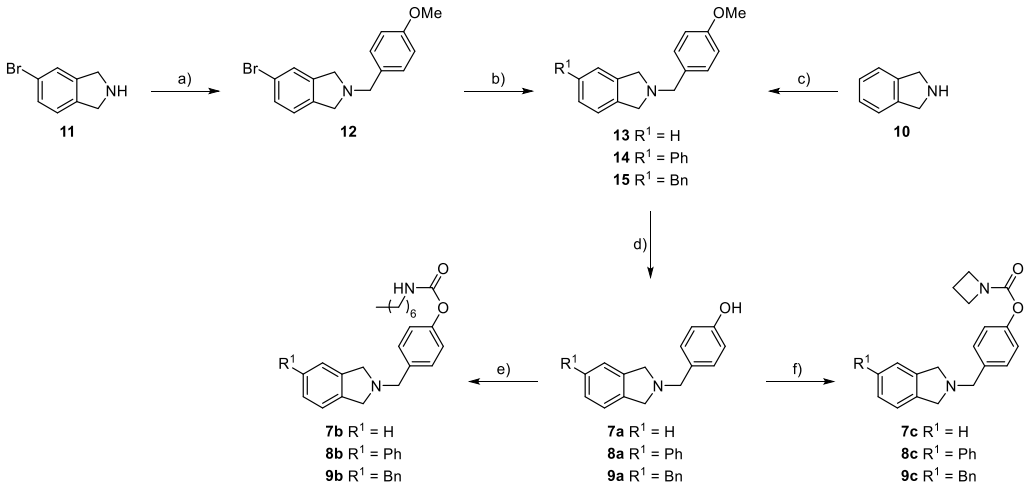

Scheme 1. Synthesis of isoindoline carbamates. Reactions and conditions: a) 1-(chloromethyl)-4-methoxybenzene, NaH, DMF, rt, 16 h, 51 %; b) K_2CO_3, Pd(ddpf)Cl_2, PhBpin or BnBpin, acetone/water, 100 °C, 30 min, 70–75 %; c) benzyl chloride, NaH, DMF, rt, 16 h, 86 %; d) BBr_3 in CH_2Cl_2, CH_2Cl_2, 0°C-rt, 1 h, 74–83 %; e) $C_7H_{15}CNO$, Et_3N, CH_2Cl_2, rt, 16 h, 20–45 %; f) 4-nitrophenyl azetidine-1-carboxylate, Cs_2CO_3, DMF, 55 °C, 16 h, 21–33 %.

phenols. For heptyl carbamates, heptyl isocyanate was used to yield target compounds **7b**, **8b**, and **9b.** Azetidine carbamates **7c**, **8c**, and **9c** were formed utilizing 4-nitrophenyl azetidine-1-carboxylate (Scheme 1).

2.2. Enzyme inhibition

Subsequently, the synthesized compounds were tested for their ChE inhibitory activity using the colorimetric Ellman's assay and the respective human enzymes (Table 1). The results demonstrate that all carbamates are active on ChEs. Overall, azetidine carbamates display higher inhibitory activity on both enzymes, *h*BChE and *h*AChE, compared to the corresponding heptyl carbamates. For example, azetidine carbamate **8c** has IC_{50} values of 25 nM on *h*BChE and 4.9 nM on *h*AChE, while its heptyl derivative **8b** has values of 1.65 μM and 374 nM, respectively. A comparison of the different isoindoline scaffolds revealed that isoindolines substituted with aromatic moieties exhibit significantly lower selectivity over *h*AChE. These findings are reflected in a selectivity index (SI) of 3.5 for compound **9c** and higher activities of inhibitors **8b**, **8c** and **9b** on *h*AChE than on *h*BChE with SIs ranging from 0.20 to 0.65. In contrast, unsubstituted isoindolines **7b** and **7c** possess a 13-fold and 5.4-fold lower activity on *h*AChE. Phenyl-substituted isoindoline **8b** shows relatively low inhibitory activity at *h*BChE, with an IC_{50} value of 1.65 μM. In contrast, non- and benzyl-substituted isoindolines **7b** and **9b** show values of 69 nM and 72 nM, respectively. Since carbamate transfer onto the enzymes' active sites results in formation of the corresponding phenols, the inhibitory activity of compounds **7a**, **8a** and **9a** were also tested on both ChEs. Except for **9a**, with an IC_{50} of 1.56 μM for *h*BChE, no IC_{50} below 2.5 μM could be determined for all phenols tested on *h*ChEs. Overall, compounds **7b** and **7c** were the

Table 1
S1R and *h*ChE *in vitro* data of isoindoline derivatives.[a]

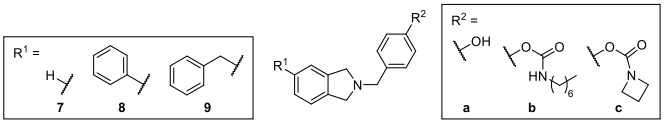

	*h*BChE IC_{50} (pIC_{50}±SEM)	*h*AChE IC_{50} (pIC_{50}±SEM)	SI (IC_{50} (*h*AChE)/IC_{50} (*h*BChE))	S1R % inhibition at 100 nM, IC_{50} (pIC_{50}±SEM)	S1R–BiP dissociation EC_{50} (pEC_{50}±SEM)
7a	>2500 nM (<3.4)	>2500 nM (<3.4)	n.d.	80 % 20 nM (7.7 ± 0.04)	118 nM (6.9 ± 0.05)
7b	69 nM (7.2 ± 0.04)	904 nM (6.0 ± 0.09)	13	41 %	316 nM (6.5 ± 0.05)
7c	37 nM (7.4 ± 0.02)	201 nM (6.6 ± 0.09)	5.4	82 % 19 nM (7.7 ± 0.05)	46 nM (7.3 ± 0.04)
8a	>2500 nM (<3.4)	>2500 nM (<3.4)	n.d.	86 %	98 nM (7.0 ± 0.02)
8b	1650 nM (5.8 ± 0.16)	374 nM (6.4 ± 0.10)	0.23	76 %	77 nM (7.1 ± 0.02)
8c	25 nM (7.6 ± 0.05)	4.9 nM (8.3 ± 0.46)	0.20	73 %	329 nM (6.5 ± 0.05)
9a	1560 nM (5.8 ± 0.05)	>2500 nM (<3.4)	>1.6	77 %	58 nM (7.2 ± 0.03)
9b	72 nM (7.1 ± 0.04)	47 nM (7.3 ± 0.08)	0.65	70 %	197 nM (6.7 ± 0.04)
9c	3.7 nM (8.4 ± 0.14)	13 nM (7.9 ± 0.09)	3.5	41 %	14 nM (7.9 ± 0.06)
Tacrine	0.052 μM (7.3 ± 0.02)	0.123 μM (6.91 ± 0.04)	2.4	n.d.	n.d.
PRE-084	n.d.	n.d.	n.d.	44 % 253 nM (6.6 ± 0.05)	426 nM (6.4 ± 0.02)

[a] n.d. not determined. Inhibition on *h*ChE was determined as triplicates after 20 min of incubation using the Ellman's assay. IC_{50} values were calculated through a sigmoidal regression using GraphPad Prism 10 [27,53,60]. Tacrine was used as (reversible) positive control [61,62]. S1R affinity was measured by displacement of radioligand [^{3}H](+)-pentazocine using membranes prepared from Wistar rat liver [63–65]. **PRE-084** was used as positive control [66]. S1R–BiP dissociation was measured in S1R-overexpressing CHO cells by immunoprecipitation using a S1R-GFP tag and BiP dosage by Elisa [67]. **PRE-084** was used as positive control [68].

most suitable for our application due to their selective *h*BChE inhibition with low IC_{50} values of 69 nM and 37 nM, and selectivity over *h*AChE with SI values of 5.4 for azetidine carbamate **7c** and a higher SI of 13 for **7b** promoted by its heptyl residue (Table 1).

2.3. Sigma-1 receptor binding and activity

Evaluation of S1R affinity was conducted through [^{3}H](+)-pentazocine radioligand binding studies using a membrane preparation from male Wistar rat liver (Table 1) [63–65]. Displacement of radioligand was quantified at a drug concentration of 100 nM. All of the carbamates synthesized, as well as their corresponding phenols occurring after enzymatic carbamate cleavage, showed affinity for S1R. The high affinities of phenols **7a**, **8a** and **9a** with 80 %, 86 % and 77 % displacement at 100 nM may be attributed to additional hydrogen bonding by the free hydroxy group. Regarding the different carbamate residues, no clear trend of S1R affinity for one carbamate over another is obvious. Here, the values of radioligand replacement reach from 41 % to 82 %. This may be explained by inversion of the ligand pose due to the different sizes of the carbamate residues for isoindoline scaffolds **8** and **9**. Also comparison of the different isoindoline scaffolds shows no clear trend, which as well could be due to different ligand orientations within one carbamate group. Among the non-substituted isoindolines, azetidine carbamate **7c** has the highest affinity for S1R, with 82 % displacement at 100 nM, whereas heptyl carbamate **7b** only displaces 41 % at the same concentration.

Phenyl-substituted scaffolds **8b** and **8c** possess similar affinity values with 76 % and 73 % displacement at 100 nM, respectively. For the 5-benzyl-substituted isoindolines, heptyl carbamate **9b** demonstrates 70 % displacement of radioligand, while azetidine **9c** shows a much lower value of 41 % (Table 1). Overall, the affinities of the compounds surpass the ones of blarcamesine (ANAVEX2-73), a S1R agonist currently in phase III study for AD that showed an IC_{50} value of 869 nM in these binding studies [50,69].

The compounds' efficacy on the dissociation of the S1R–BiP complex was determined using an immunoprecipitation assay followed by ELISA. The assay was performed on S1R-expressing Chinese hamster ovarian (CHO) cells (Table 1). All isoindoline derivatives result in the dissociation of the S1R–BiP complex. Therefore, the compounds can be regarded as S1R agonists [36].

Based on the above discussed *in vitro* results, azetidine carbamate **7c** represents the ideal prototype for the desired dual-acting functions and was therefore further investigated. In addition, its corresponding cleavage product and S1R agonist **7a** was evaluated to determine whether or to which extent it may contribute to the overall pharmacological effects of compound **7c** after carbamate transfer. To assess the benefit of the dual-target strategy in comparison to corresponding single-target approaches, we also included the selective *h*BChE inhibitor **7b** as a comparator.

2.4. hBChE inhibition mode determined by kinetic investigations

Regarding the mode and mechanism of *h*BChE inhibition, we assumed a pseudo-irreversible one for the carbamate inhibitors, consisting of three steps (Table 2): (i) Formation of a reversible enzyme-phenolcarbamate complex (EPC) between the enzyme (E) and the inhibitor (PC) described by equilibrium constant K_i. (ii) Transfer of the carbamate moiety to the enzymes active site (EC) under release of the corresponding phenol (P) with k_3 representing the carbamylation rate constant. (iii) Reconstitution of enzyme activity through hydrolysis resulting in the release of carbamate (C') and free enzyme (E) characterized by velocity constant k_4. Decarbamylation typically occurs much more slowly than carbamylation, so k_4 is lower than k_3 (Table 2) [60]. To ascertain this inhibition mode, enzyme kinetics for *h*BChE inhibitors **7b** and **7c** were investigated (Fig. 4). On-kinetic was assessed by varying incubation times, ranging from 5 min to 60 min for a series of inhibitor concentrations (Fig. 4a).

Table 2
Kinetic values of carbamates (PC) **7b** and **7c** for pseudo-irreversible inhibition of *h*BChE (E).[a]

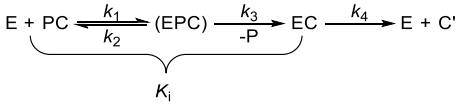

	K_i [nM]	k_3 [min^{-1}]	k_3/K_i [min^{-1} μM^{-1}]	$t_{1/2}$ [h]	k_4 [h^{-1}]
7b	2026 ± 834	2.22 ± 0.807	1.09 ± 0.602	2.6	0.269 ± 0.028
7c	579 ± 117	1.40 ± 0.195	2.42 ± 0.688	2.7	0.257 ± 0.017

[a] Enzyme (E), enzyme-phenolcarbamate complex (EPC), carbamylated enzyme (EC), corresponding phenol (P), free carbamate (C').

Time-dependent change in inhibitory activity obtained from these experiments demonstrated a covalent inhibition mode. The Michaelis-Menten kinetic (Figures S 16-18) was applied as described by Hosie *et al.* [70] and Feaster *et al.* [71], providing parameters K_i and k_3 (Table 2) [27,53,72]. In correlation to the measured IC_{50} values, compound **7c** possesses a lower K_i value of 579 nM compared to inhibitor **7b**. The carbamylation rate constant k_3 is 1.40 min^{-1} and 2.20 min^{-1} for inhibitors **7c** and **7b**, respectively. As IC_{50} values contingent upon the incubation time for covalent inhibitors, Copeland posits a time-independent metric for the effectiveness of enzyme inactivation, derived through second-order rate constant (k_3/K_i) [73]. A comparison of the second-order rate constants reveals that both carbamates demonstrate a comparable behavior, with azetidine carbamate **7c** exhibiting a marginally better value of 2.42 min^{-1} μM^{-1} due to its comparatively low K_i and slower carbamate transfer.

Reconstitution of enzyme activity via hydrolysis was determined in dilution experiments, wherein *h*BChE was incubated with high amounts of inhibitor and subsequently diluted. In the case of reversible inhibition, enzyme activity is regained immediately. In contrast, under pseudo-irreversible inhibition, the enzyme activity is reconstituted gradually due the prior requirement of hydrolysis of the covalent bond [74]. This pseudo-irreversible behavior is exhibited by both *h*BChE inhibitors **7b** and **7c** (Fig. 4b). Azetidine carbamate **7c** exhibits a half-life time of 2.7 h and a decarboxylation rate of 0.257 h^{-1} which is similar to heptyl carbamate **7b** (Table 2) with a half-life time of 2.6 h and decarboxylation rate of 0.269 h^{-1}.

2.5. Computational studies

Molecular docking studies were conducted to predict binding modes and analyze the structure-activity relationships of the chosen isoindolines **7**–**9** (Fig. 3b) on both targets. Docking was performed with Schrödinger's Glide (v10.1)[75,76], as described in detail in the Experimental Section (all docking poses and their scores can be found in the Supporting Information (Fig. S13-15), using the PDB structure 4M0E of *h*AChE (resolution 2.00 Å) and the crystal structure 6QAA of *h*BChE (resolution 1.90 Å) as in our previous work [26,72]. As carbamates are expected to act by the pseudo-irreversible inhibition mechanism described in section 2.4, a covalent tetrahedral intermediate formed by reaction with the catalytic serine was modeled. Constraints were applied between the carbonyl function of the carbamate and the backbone of the glycines forming the oxyanion hole to ensure comparable binding modes; this is based on the common mechanism of ChEs in which the nucleophilic attack of the catalytic serine on the carbonyl carbon and proton transfer to the adjacent histidine leads to formation of a covalent tetrahedral intermediate whose negative charge is stabilized by the oxyanion hole consisting of the backbone atoms of two glycines.[77]

On *h*BChE, the azetidine and heptyl chains of the carbamates are positioned in the acyl binding site, formed by Trp231, Leu286 and Val288 (Fig. 5a). More favorable docking scores for isoindolines with the

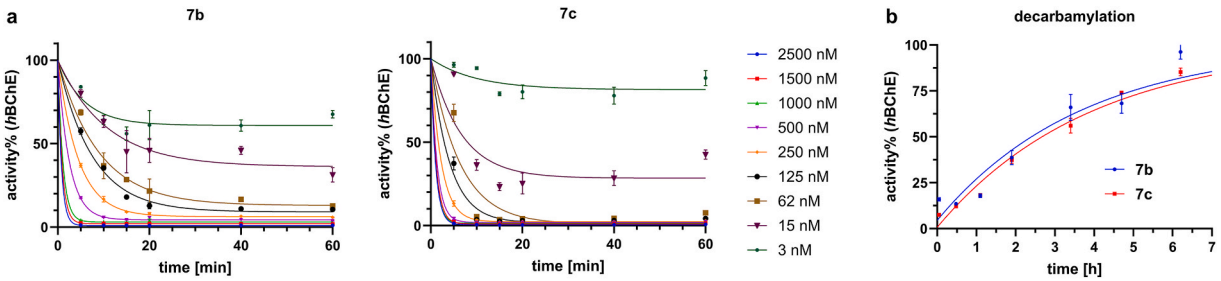

Fig. 4. (**a**) On-kinetics: Time-dependent *h*BChE inhibition of heptyl carbamate **7b** and azetidine carbamate **7c**. (**b**) Off-kinetics: Time-dependent carbamate cleavage and reconstitution of *h*BChE activity after inhibition by compounds **7b** and **7c**. Results are shown as means ± SEM of triplicates [27].

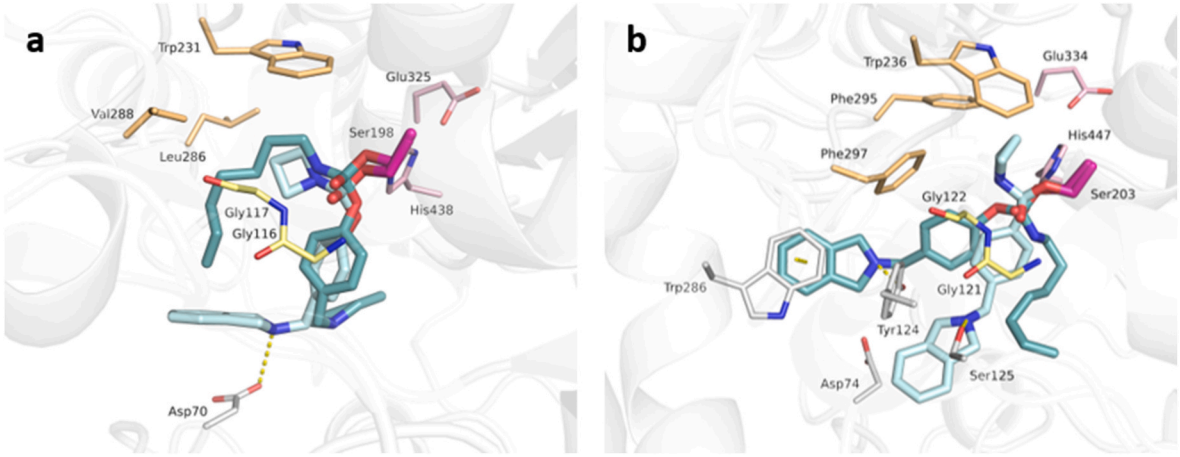

Fig. 5. Docking poses of representative isoindolines on *h*ChE. The catalytic triad is marked in pink, the oxyanion hole in yellow and the acyl binding pocket in orange. (**a**) Preferred binding mode of heptyl carbamate **7b** (light teal) and azetidine carbamate **7c** (pale cyan) on *h*BChE. (**b**) Preferred binding mode of heptyl carbamate **7b** (light teal) and azetidine carbamate **7c** (pale cyan) on *h*AChE.

same scaffold are obtained for the azetidine than for the heptyl carbamates, reflecting less steric hindrance and suggesting higher affinity, as observed *in vitro*. The isoindoline core lies in the exterior lipophilic pocket above the oxyanion hole. Here, a hydrogen bond is observed for compounds **7c**, **8c**, and **9b-c**, respectively, between the isoindoline nitrogen and Asp70, which has a crucial role for the association of positively charged ligands (Fig. 5a) [78]. This hydrogen bond is not formed by heptyl carbamates **7b** and **8b**, resulting in less favorable docking scores, suggesting reduced binding affinity, which was also observed in the binding assay. Overall, the introduction of aryl substituents in the isoindoline scaffold leads to better scores due to extended hydrophobic interactions, which matches the experimental data of azetidine carbamates **7c-9c**.

In *h*AChE, the acyl pocket formed by Trp236, Phe295 and Phe297 is much smaller compared to *h*BChE, resulting in a position of the heptyl chain of compounds **7b**, **8b** and **9b** outside of the acyl pocket, while the smaller azetidines **7c** and **9c** fit into the acyl pocket (Fig. 5b). The preference for azetidine, observed in the *in vitro* data, is also reflected in more favorable docking scores for azetidine carbamates **7c** and **8c** compared to heptyl carbamates **7b** and **8b**. Furthermore, a common binding mode can be derived by the docking results for most of the compounds, represented by a hydrogen bond that is formed between the isoindoline nitrogen and Tyr124, while the aromatic isoindoline ring promotes pi-stacking interactions with Trp286. The only exception is inhibitor **7c**, where a hydrogen bond is formed between the isoindoline nitrogen and Ser125 (Fig. 5b). Again, introduction of aromatic substituents leads to improved docking scores, providing an indicator for stronger binding. Therefore, the non-substituted isoindolines **7b** and **7c** are more favorable for selectivity over *h*AChE. Of these two carbamates, compound **7c** exhibited significantly superior docking scores for *h*BChE, making it the most suitable inhibitor for our application in terms of ChE activity.

Studies on the human S1R were conducted based on the publication of Linkens *et al.* [56] using the crystal structure 5HK1. The results show that all compounds **7–9** form the expected hydrogen bond to Glu172 through the basic amine of the isoindoline core, crucial for binding according to Glennon's model and in accordance with the obtained experimental binding data (Fig. 6) [54]. However, the isoindoline's orientation varies between ligands, which is also reflected by the different values in the radioligand binding assay. This leads to the assumption that the primary pocket is occupied by the larger substituent when the isoindoline scaffold is extended, which is illustrated in the following results.

For unsubstituted isoindolines **7a-c** the isoindoline moiety is placed in the smaller secondary pocket and the larger benzyl fragment in the primary one (Fig. 6a). The common binding mode is reflected in similar scores. A slightly improved score for azetidine **7c** compared to heptyl carbamate **7b** correlates with an expected larger loss of entropy for the sterically more demanding and flexible heptyl chain. However, for carbamate **7b**, a more significant loss of affinity was obtained *in vitro*. Phenol **7a** forms an additional hydrogen bond with Thr181, which may explain its high affinity, even though it lacks hydrophobic interactions compared to carbamates **7b**,**c** (Fig. 6a). The introduction of aromatic residues into the isoindoline scaffold, as in compounds **8a-c** and **9a-c**, generally leads to better scores due to additional hydrophobic interactions. In the radioligand binding assay, this is only reflected for compound **8a**. For phenols **8a** and **9a**, a reversed orientation of the isoindoline compared to phenol **7a** is predicted, with the larger aromatic

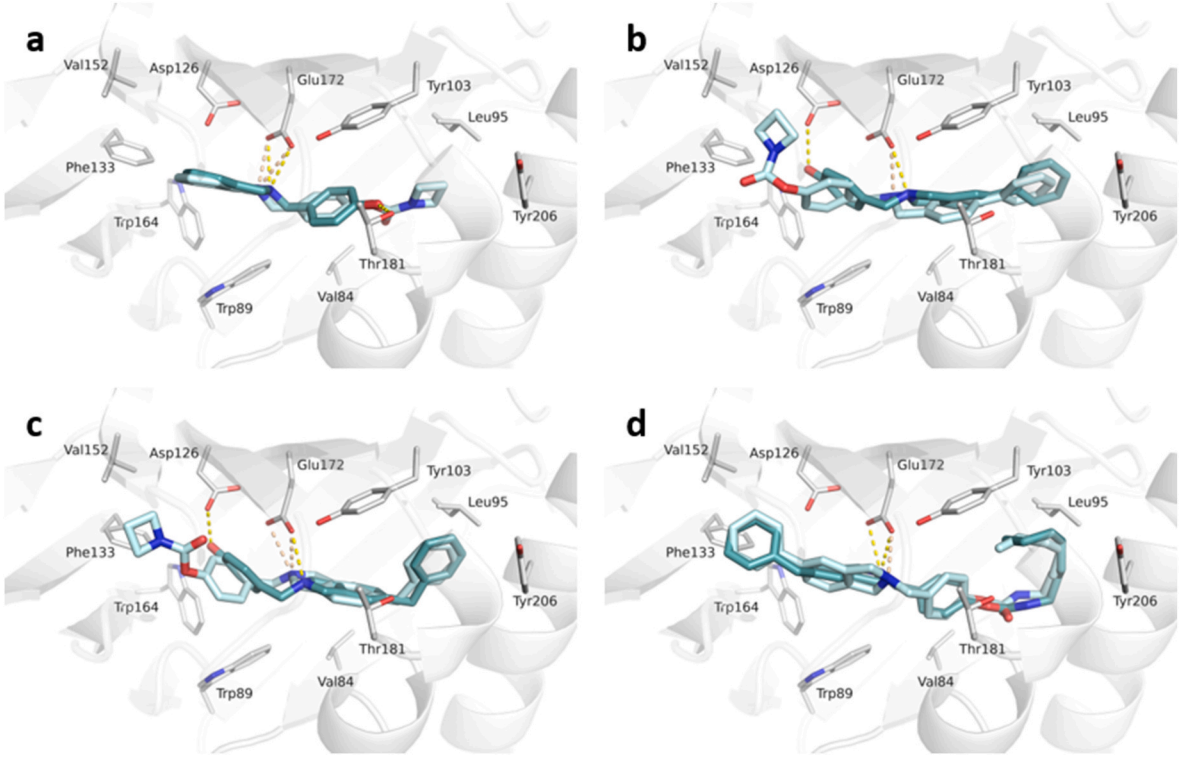

Fig. 6. Docking poses of representative isoindolines on the human S1R. (**a**) Preferred binding mode of azetidine carbamate **7c** (pale cyan) and its phenol **7a** (light teal). (**b**) Preferred binding mode of azetidine carbamate **8c** (pale cyan) and its phenol **8a** (light teal). (**c**) Preferred binding mode of azetidine carbamate **9c** (pale cyan) and its phenol **9a** (light teal). (**d**) Preferred binding mode of heptyl carbamates **8b** (pale cyan) and **9b** (light teal).

substituent placed into the primary hydrophobic pocket (Fig. 6b and c). Moreover, phenols **8a** and **9a** form a hydrogen bond between the phenol group and Asp126, which explains the observed high affinities in the radioligand binding assay (Fig. 6b and c). Azetidines **8c** and **9c** exhibit a similar orientation as the respective phenols **8a** and **9a** (Fig. 6b and c), whereas the heptyl derivatives **8b** and **9b** exceed the capacity of the smaller secondary pocket (Fig. 6d). This leads to an inverted orientation, with the carbamate moiety in the primary pocket and, in contrast to the experimental data, poorer scores compared to azetidine carbamates **8c** and **9c**. Despite more favorable docking scores of aromatic substituted isoindolines **8a-c** and **9a-c** compared to non-substituted isoindolines **7a-c**, the docking scores of compounds **7a-c** also indicate binding, as demonstrated *in vitro* for compounds **7a** and **7c**. In summary, compound **7c** exhibits the most favorable score profile over the investigated targets, which is also reflected in the compound's experimental data.

2.6. Lack of neurotoxicity and solubility

For the subsequent *in vivo* studies envisaged, we then tested for potential neurotoxicity of the compounds, as well as their aqueous solubility. Neurotoxicity was assessed in an MTT assay using HT22 cells treated with hybrid molecules **7b**, **7c** or their corresponding cleavage product **7a**. No toxicity was observed for hybrid compound **7c** or its cleavage product **7a** up to a concentration of 100 μM. Inhibitor **7b** displayed only slight toxicity at a high concentration of 75 μM, a level not reached in our subsequent *in vivo* studies (Fig. 7). To enable the solubility of the compounds for *in vivo* application, the HCl salts were prepared and their solubility in phosphate-buffered saline (PBS) buffer was determined using the continuous shake protocol.[79] Samples were analyzed by high-performance liquid chromatography (HPLC) and the solubility was calculated by UV quantification (Table 3). In accordance with their design, the azetidine carbamate **7c·HCl** showed a higher solubility of 82 μg/mL compared to ligand **7b·HCl** with 1.7 μg/mL, while the free phenol **7a·HCl** with 84 μg/mL had a similar solubility to carbamate **7c·HCl** in PBS buffer (Table 3).

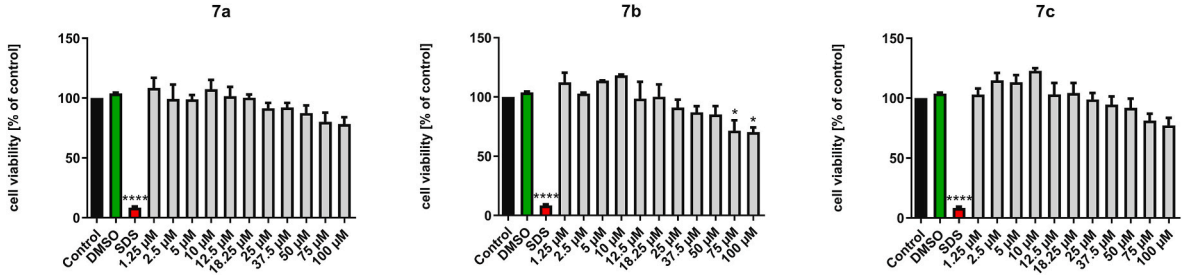

Fig. 7. Lack of neurotoxicity of **7a-c** in MTT assay using neuronal HT22 cells. Results are shown as means ± SEM of three independent experiments. Viability of treated cells were compared with untreated control cells (100 %). ANOVA: $F_{(13,28)} = 18.49$; $p < 0.0001$ (**7a**); $F_{(13,25)} = 16.2$; $p < 0.0001$ (**7b**), $F_{(13,28)} = 23.0$; $p < 0.0001$ (**7c**). Levels of significance: $^{*}p < 0.05$, $^{****}p < 0.0001$.

Table 3
Solubility in PBS buffer of HCl salts of compounds tested *in vivo*.[a]

	Solubility [μg/mL] ± SEM
7a·HCl	84 ± 1.8
7b·HCl	1.7 ± 0.13
7c·HCl	82 ± 3.9

[a] Solubility in PBS measured using the continuous shake protocol.[79] Samples were measured as triplicates.

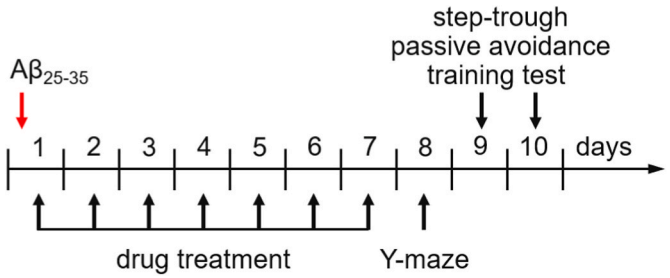

Fig. 8. Schematic application protocol for Aβ mouse model. The $A\beta_{25\text{-}35}$ peptide is injected ICV (9 nmol/mouse) on day 1. Compounds are administered IP once daily between days 1 and 7. The spontaneous alternation test is performed on day 8, passive avoidance training on day 9 and retention test on day 10. Adapted from Carles *et al.* [67].

2.7. *In vivo* studies

The *in vivo* neuroprotective effects of compounds **7a**, **7b** and **7c** were evaluated in our established Aβ mouse model, as previously described for S1R agonists and BChE inhibitors alike (Fig. 8) [28,53,68].

Swiss-OF1 mice were administered oligomeric $A\beta_{25\text{-}35}$ peptide intracerebroventricularly (ICV) and treated intraperitoneally (IP) with the test compounds. The short-term memory of the mice was tested using spontaneous alternation in the Y-maze. Effects on long-term memory were assessed using the step-through type passive avoidance test. Treatment with the *h*BChE inhibitor **7b** resulted in a significant and bell-shaped prevention of $A\beta_{25\text{-}35}$-induced spontaneous alternation impairment in the 0.1–3 mg/kg dose range (Fig. 9a), but only at the lowest dose, it prevented $A\beta_{25\text{-}35}$-induced passive avoidance deficit (Fig. 9b).

Compounds **7c** and **7a** show parallel bell-shaped effects on both memory tests but with a clear difference in their active dose range: Dual-target compound **7c** was active at 0.01–0.1 mg/kg (Fig. 9c and d) while its corresponding cleavage product and S1R agonist **7a** was still considerably, albeit less active at 0.3–1 mg/kg (Fig. 9e and f). The observation that the dual-target compound **7c** was active in a 10-fold lower range suggests additive or synergistic effect by addressing both targets simultaneously.

In order to prove involvement of BChE inhibition in the hybrids' *in vivo* effect, compound **7c** and its cleavage product **7a** were tested in BChE KO

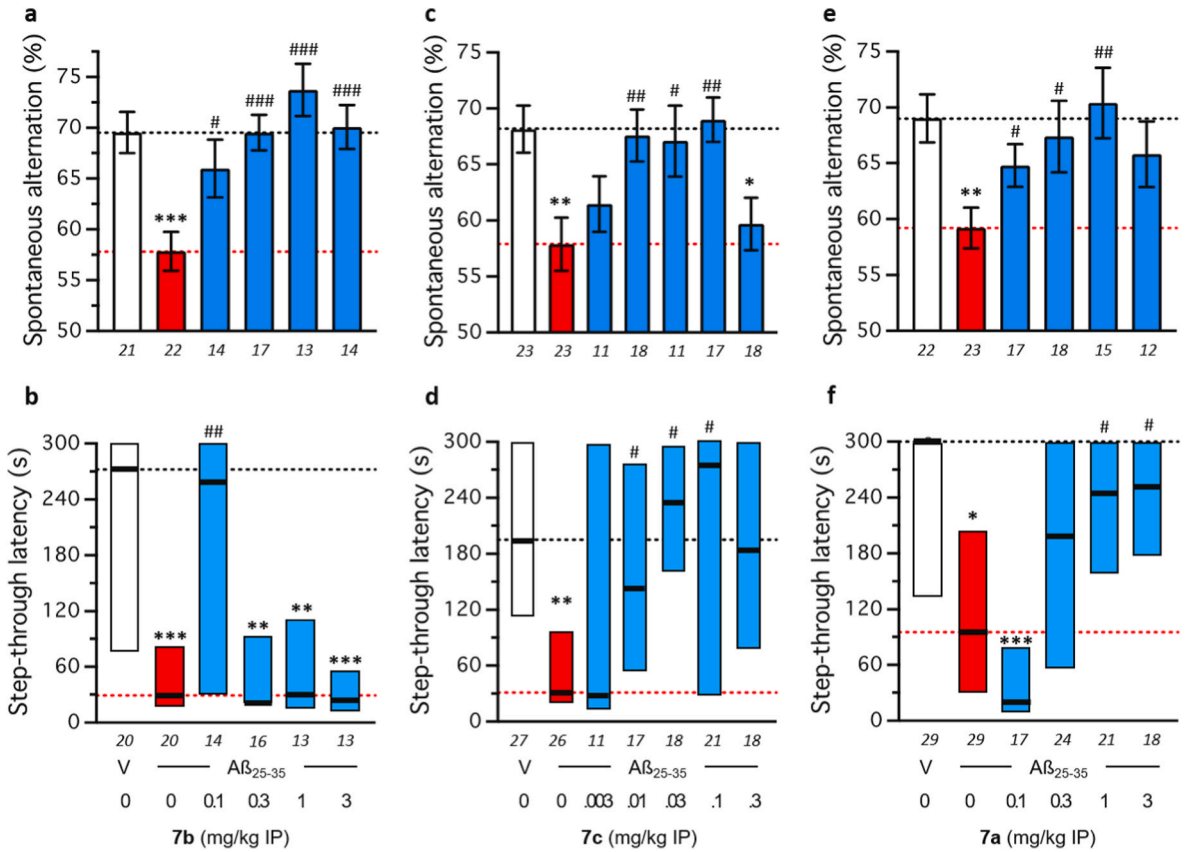

Fig. 9. Effects of (**a**, **b**) compounds **7b**, (**c**, **d**) **7c**, and (**e**, **f**) **7a**, respectively, on $A\beta_{25\text{-}35}$ induced learning impairments in mice. (**a**, **c**, **e**) Spontaneous alternation performance in the Y-maze and (**b**, **d**, **f**) retention latency in the passive avoidance test. Mice were treated with $A\beta_{25\text{-}35}$ (9 nmol, ICV) or vehicle (3 μL of ddH_2O, V) on day 1, then received either vehicle (dimethyl sulfoxide (DMSO) 10 % in saline) or the compound (0.003–0.3 or 0.1–3 mg/kg) IP between day 1–7. Mice were then tested for spontaneous alternation on day 8 and passive avoidance on day 9 (training) and day 10 (test). Group size is shown beneath each bar graph. Data show ± SEM (**a**, **c**, **e**) or median and interquartile range (**b**, **d**, **f**). ANOVA: $F_{(5,95)} = 7.053$; $p < 0.0001$ in (**a**); $F_{(6,114)} = 4.064$; $p = 0.0010$ in (**c**); $F_{(5,101)} = 2.909$; $p = 0.0170$ in (**f**); Kruskal Wallis ANOVA: H = 25.83; $p < 0.0001$ in (**b**), H = 13.86, $p = 0.0312$ in (**d**), H = 21.65, $p = 0.0006$ in (**f**). $^{*}p < 0.05$, $^{**}p < 0.01$, $^{***}p < 0.001$ vs V-treated group; $\#p < 0.05$, $\#\#p < 0.01$, $\#\#\#p < 0.001$ vs $A\beta_{25\text{-}35}$-treated group; Dunnett's test in (**a**, **c**, **e**); Dunn's test in (**b**, **d**, **f**).

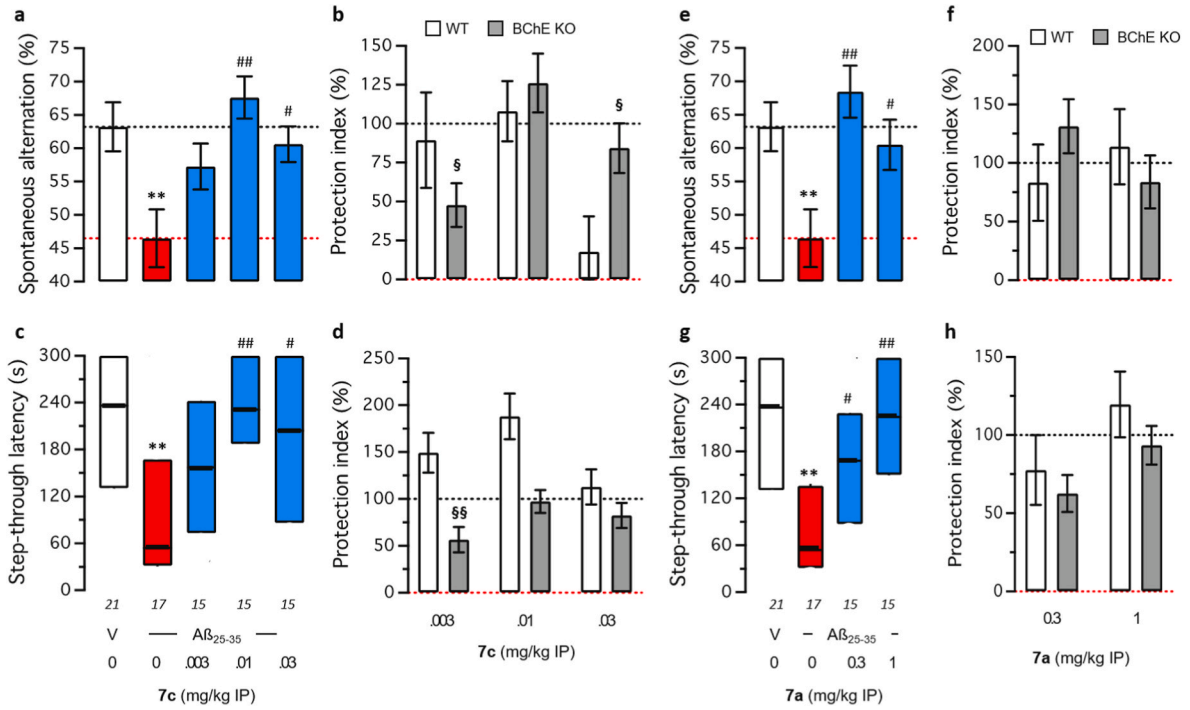

Fig. 10. Effects of (**a**–**d**) compounds **7c** and (**e**–**h**) **7a** on $A\beta_{25\text{-}35}$ induced learning impairments in BChE KO mice. (**a**, **e**) Spontaneous alternation performance in the Y-maze and (**c**, **g**) retention latency in the passive avoidance test. In (**b**, **d**, **f**, **h**) data are presented as protection index, calculated using the V/V-treated group as 100 % and $A\beta_{25\text{-}35}$/V-treated group as 0 %. White columns show the data from WT mice (Fig. 9) and grey column from BChE KO mice (this figure). Mice were treated with $A\beta_{25\text{-}35}$ (9 nmol, ICV) or vehicle (3 μL of ddH_2O, V) on day 1, then received either vehicle (DMSO 10 % in saline) or the compound (0.003–0.03 or 0.3–1 mg/kg) IP between day 1–7. Mice were then tested for spontaneous alternation on day 8 and passive avoidance on day 9 (training) and day 10 (test). Group size is shown beneath each bar graph in (**a**, **c**, **e**, **g**). Data show ± SEM or median and interquartile range (**c**, **g**). ANOVA: $F_{(4,46)} = 5.055$; $p = 0.000–18$ in (**a**); $F_{(3,38)} = 5.786$; $p = 0.0023$ in (**c**); Kruskal Wallis ANOVA: H = 13.48; $p = 0.0091$ in (**c**), H = 15.50, $p = 0.0014$ in (**g**). $^{**}p < 0.01$ vs V/V-treated group; $\#p < 0.05$, $\#\#p < 0.01$ vs $A\beta_{25\text{-}35}$/V-treated group; $\S p < 0.05$, $\S\S p < 0.01$ vs. WT data; Dunnett's test in (**a**, **b**, **e**); Dunn's test in (**c**, **d**, **g**).

mice (Fig. 10) using the same $A\beta_{25\text{-}35}$ induced neurotoxicity protocol as described above. Preliminary Western blot analyses showed that BChE KO mice do not exhibit any altered S1R expression in both hippocampus or cortex compared to their wild-type littermates. Dose–response data for hybrid molecule **7c** obtained in BChE KO mice was then compared with the protective effects observed in wild-type Swiss OF1 mice (Fig. 10a–d). The spontaneous alternation exhibited a rightward shift in the bell-shaped dose-response curve (Fig. 10b), while the passive avoidance assay revealed a global attenuation of the effect (Fig. 10d). Overall, hybrid compound **7c** exhibited a reduction in efficacy, yet its S1R component remained active. In contrast, selective S1R compound **7a** demonstrated equivalent activity in both wild type (WT) and BChE KO mice (Fig. 10e–h). The lack of effect of compound **7c** in BChE KO mice confirmed the involvement of BChE inhibition for the overall neuroprotective effect of the compound.

To test the hypothesis of synergism between the two targets, we combined reference ligands selective for each target and tested their neuroprotective efficiency using the two behavioral procedures (Fig. 11). We used the isobologram representation of two-drugs combination as previously described [80–84]. We utilized cutamesine (**SA4503**) as S1R agonist [48], and **UW-MD-95** as BChE inhibitor [28], and briefly confirmed their dose-response effect in the 0.3–1 mg/kg IP dose-range (Fig. 11a and b) to define their highest non-active dose and lowest active dose. These doses were combined and the level of protection calculated in percentage of controls (V- or $A\beta_{25\text{-}35}$-treated groups, Fig. 11c and d). The combination index was calculated (see Supplementary Table S1) and a synergistic neuroprotective effect was observed in 4 out of 6 readouts, with synergism particularly pronounced in long-term memory (Fig. 11b and d). This confirmed that compound **7c** addressed both pharmacological targets acting synergistically and resulting in a very low active dose-range compared to selective ligands such as compounds **7b** and **7a**. Furthermore, these observations

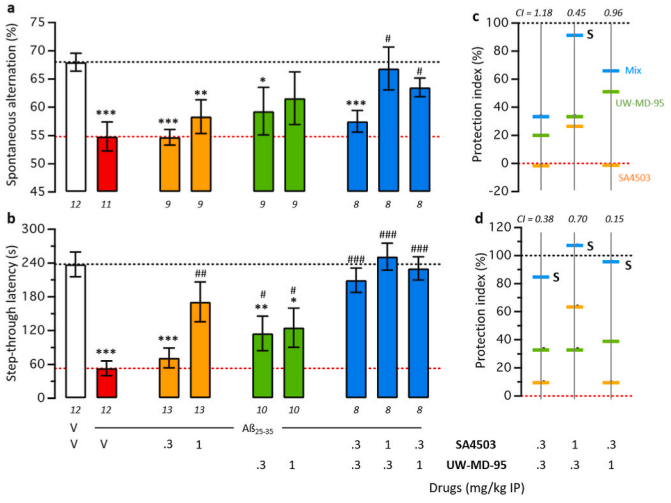

Fig. 11. Combination studies between cutamesine (**SA4503**) and **UW-MD-95** in $A\beta_{25\text{-}35}$-treated mice. (**a**) Spontaneous alternation performance in the Y-maze; (**b**) retention latency in the passive avoidance test. Mice were treated with $A\beta_{25\text{-}35}$ (9 nmol, ICV) or vehicle (3 μL of ddH_2O, V) on day 1, then received either vehicle (DMSO 10 % in saline) or the compound (0.3–1 mg/kg) IP between day 1–7. Mice were then tested for spontaneous alternation on day 8 and passive avoidance on day 9 (training) and day 10 (test). (**a**, **b**) show mean ± SEM used for calculations and the group size is shown below each bar graph. ANOVA: $F_{(8,73)} = 3.087$, $p = 0.0047$, in (**a**); H = 44.72, $p < 0.0001$, in (**b**). $^{*}p < 0.05$, $^{**}p < 0.01$, $^{***}p < 0.001$ vs. V-treated group; $\#p < 0.05$, $\#\#p < 0.01$, $\#\#\#p < 0.001$ vs. $A\beta_{25\text{-}35}$-treated group; Dunnett's test in (**a**); Dunn's test in (**b**). (**c**, **d**) Protection is shown using a cursor-on-scale representation, with data from V-treated group as 100 % and from $A\beta_{25\text{-}35}$-treated group as 0 %. Calculated protection indexes are shown. S: synergic effect, with combination index combination index (CI) < 1.

highlight the high therapeutic potential of such hybrid molecules.

3. Conclusions

In this work, isoindoline-based small molecules were designed and could be synthesized in a four-step procedure. Their structure-activity relationships on *h*BChE, *h*AChE and S1R, respectively, were evaluated. Compound **7c** was identified as a dual-acting ligand, inhibiting *h*BChE and activating S1R in two-digit nanomolar "balanced" concentrations, *i.e.*, interacting with both molecular targets in the same concentration range, a property that is not often reached in hybrid molecule design. The activities achieved are remarkably high compared to previously reported dual-target compounds targeting *h*BChE, which are usually active in the micromolar range [16,17]. Compared to compound **7c**, compounds **7b** and **7a** were found to act only on one of the two aspired targets. Due to the structural similarity of all three compounds, single-targeting ligands **7b** and **7a** provided excellent references for evaluation of dual-target ligand **7c** and were thus also investigated further. Kinetic investigations confirmed the expected pseudo-irreversible inhibition mode of carbamates **7b** and **7c**, with half-lives of 2.6 h and 2.7 h, respectively, enabling longer target engagement compared to reversible inhibitors. Binding data can be explained and illustrated by molecular docking studies on the targets. Prior to *in vivo* studies, all three compounds were tested for neurotoxicity on HT22 cells and concentrations up to 50 μM did not elicit any neurotoxic effects. Finally, the three candidates were administered *in vivo* using an established AD mouse model. All compounds demonstrated the ability to mitigate $A\beta_{25\text{-}35}$ induced learning impairments. In spontaneous alternation, the single-target ligands **7b** and **7a** showed an effect at a dosage of 0.1 mg/kg. In contrast, dual-acting ligand **7c** possessed an even 10-fold lower effective dose, with a very low dosage of 0.01 mg/kg. This dose is remarkably low even compared to other multi-target directed ligands addressing neuroinflammation like the clinically investigated S1R agonist blarcamesine (10–30 mg/kg) [50], the S1R agonist and *h*AChE inhibitor donepezil (0.5–1 mg/kg) [47], or our reported benzimidazole BChE inhibitor and cannabinoid-receptor 2 agonist (0.3–3 mg/kg) [53]. Furthermore, combinational studies with S1R agonist **SA4503** and *h*BChE inhibitor **UW-MD-95** demonstrated that the very low required dosage of hybrid compound **7c** is due to the (expected) synergistic effect by targeting both *h*BChE and S1R concurrently.

However, some limitations of hybrid molecule **7c** should also be acknowledged: Although the compound displays an unambiguous dual-targeting profile, its selectivity over *h*AChE is only quite moderate compared to our previously described *h*BChE inhibitors, which might be relevant for potential side effects in a therapeutic context. In addition, the compound showed only moderate solubility, and its full ADME profile has not yet been determined. These aspects need to be addressed in the next stages of compound development. Ongoing studies in transgenic mouse models will further elucidate the long-term efficacy and safety profile of hybrid **7c**. Overall, this study underscores the potential of low-molecular-mass hybrid compounds targeting *h*BChE and the S1R as a promising avenue to combat the multifactorial nature of neurodegenerative diseases such as AD.

4. Experimental section

4.1. Chemistry

4.1.1. General information and procedures

All reagents were purchased from Sigma Aldrich (St. Louis, Missouri), ABCR (Karlsruhe, Germany), and BLDpharm (Shanghai, China), enamine (Kyiv, Ukraine) and used without further purification. Tetrahydrofuran (THF) was dried by refluxing over sodium under an argon atmosphere. DMF and CH_2Cl_2 used as reaction solvents were purchased as dry solvents with safe seal (Sigma-Aldrich, St. Louis, Missouri) and used under argon atmosphere. Thin-layer chromatography was performed on silica gel 60 alumina foils with a fluorescent indicator (254 nm) (Macherey Nagel GmbH & Co. KG, Düren, Germany). Spots were detected by UV light (254 and 366 nm) or through staining with ninhydrin or $KMnO_4$. Normal phase purification was performed using a silica gel with a particle size of 40–63 μm (Macherey Nagel GmbH & Co. KG, Düren, Germany) as stationary phase and PE/EtOAc or CH_2Cl_2/MeOH as liquid phase with optional addition of 1 % Et_3N. Reverse phase purification was performed using flash column chromatography with C18 silica gel with 30 μm particle size (Büchi, Flawil, Switzerland) as stationary phase and water/MeOH with 0.1 % FA or water/MeCN with 0.1 % FA as liquid phase. Nuclear magnetic resonance (NMR) spectra were measured with a Bruker AV-400 NMR instrument (Bruker, Karlsruhe, Germany) in deuterated solvents (DMSO; $CDCl_3$, CD_3OD, D_2O). Chemical shifts are expressed in parts per million (ppm) relative to the respective solvent residues. Purity was determined by HPLC (Shimadzu Products), containing a DGU-20A3R degassing unit, a LC20AB solvent delivery unit, and a SPD-20A UV/VIS detector. UV detection was measured at 254 nm. Mass spectra were obtained by a liquid chromatography-mass spectrometry (LCMS) 2020 (Shimadzu Products). As a stationary phase, a Synergi 4U fusion-RP (150 mm × 4.6 mm) column (Synergi, Aschaffenburg, Germany) was used, and as a mobile phase, a gradient of H_2O/MeOH with 0.1 % FA was used. Parameters: A = water, B = MeOH, V(B)/[V(A) + V(B)] = from 5 to 90 % over 10 min, V(B)/[V(A) + V(B)] = 90 % for 5 min, and V(B)/[V(A) + V(B)] = from 90 to 5 % over 3 min. The method was performed with a flow rate of 1.0 mL/min. All compounds used in biological evaluation were ≥95 % pure by HPLC [27,53].

General procedure for benzyl substitution (GP-A). Isoindoline (**10**) (1.0 eq.) was dissolved in DMF (0.7 M). NaH (1.2 eq., 60 %) and 1-(Chloromethyl)-4-methoxybenzene (1.2 eq.) were added successively. The reaction mixture was stirred at rt for 2 h. The reaction was terminated by the addition of water. The aquatic layer was extracted with EtOAc. The combined organic layers were dried over Na_2SO_4, filtered and the solvent was removed under reduced pressure. The product was obtained and used without further purification.

General procedure for suzuki coupling (GP-B). 5-Bromoisoindoline (**11**) (1.0 eq.) was dissolved in acetone/H_2O (3:1, 0.2 M) in an argon flushed reaction tube. K_2CO_3 (3.0 eq.), $Pd(dppf)Cl_2$ (10 mol%) and the respective boronic acid pinacol ester (1.5 eq.) were added successively. The reaction mixture was stirred at 100 °C for 30 min. The reaction was terminated by the addition of KOH (1 M). The organic layer was extracted with CH_2Cl_2. The combined organic layers were washed with brine, dried over Na_2SO_4, filtered and the solvent was removed under reduced pressure.

General procedure for methyl ether cleavage (GP-C). Ether (1.0 eq.) was dissolved in CH_2Cl_2 (0.1 M) and BBr_3 (4.0 eq., 1 M in CH_2Cl_2) was added dropwise. The reaction mixture was warmed up to rt and stirred for 1 h. The reaction was terminated by the addition of sat. aq. $NaHCO_3$. The aquatic layer was extracted with CH_2Cl_2. The combined organic layers were dried over Na_2SO_4, filtered and the solvent was removed under reduced pressure. The crude product was obtained and used without further purification.

General procedure for heptyl carbamate formation (GP-D). Phenol (1.0 eq.) was dissolved in CH_2Cl_2 (0.04 M), heptyl isocyanate (1.5 eq.) and Et_3N (1.5 eq.) were added successively. The reaction mixture was stirred at rt for 16 h. The solvent was removed under reduced pressure and the crude product was loaded onto celite. The product was obtained after purification by reverse phase flash column chromatography.

General procedure for azetidine carbamate formation (GP-E). Phenol (1.0 eq.) was dissolved in DMF (0.02 M), Cs_2CO_3 (2.0 eq.) and 4-nitrophenyl azetidine-1-carboxylate (2.0 eq.) were added successively. The reaction mixture was stirred at 55 °C for 16 h. The reaction was terminated by the addition of water. The aquatic layer was extracted with EtOAc. The combined organic layers were washed with brine, dried over Na_2SO_4, filtered and the solvent was removed under reduced pressure. The product was obtained after purification by reverse phase flash column chromatography.

General procedure for HCl-salt formation (GP-F). Amine (1.0 eq.) was dissolved in THF (0.8 M). HCl dissolved in Et_2O (1.5 eq., 1 M) was added dropwise. The reaction was stirred at rt for 1 h. The solvent was removed under reduced pressure, the precipitate was washed with Et_2O and dried under reduced pressure. HCl salts were obtained in quantitative yields.

4.1.2. Synthesis and characterization of compounds

4.1.2.1. 5-Bromo-2-(4-methoxybenzyl)isoindoline (12). Compound **12** was synthesized according to GP-A from 5-bromoisoindoline (**11**). The product **12** (2.88 g, 9.07 mmol, 71 %) was obtained as a brown solid after purification by column chromatography (CH_2Cl_2/MeOH 0–1 % + 0.5 %Et_3N). **^{1}H NMR** (400 MHz, $CDCl_3$) $\delta = 7.30$ (dt, $J = 3.3$, 4.4 Hz, 4H), 7.03 (d, $J = 8.4$ Hz, 1H), 6.89 (d, $J = 8.6$ Hz, 2H), 3.88 (s, 2H), 3.85 (s, 2H), 3.83 (s, 2H), 3.82 (s, 3H) ppm. **^{13}C NMR** (101 MHz, $CDCl_3$) $\delta = 58.9$, 142.8, 139.4, 131.0, 130.0, 129.8, 125.7, 124.0, 120.4, 113.9, 59.5, 58.5, 58.4, 55.4 ppm. **ESI-MS:** *m/z* calculated for $[M+H]^+$: 318.04, found: 318.05. **mp** = 89 °C.

4.1.2.2. 2-(4-Methoxybenzyl)isoindoline (13). Compound **13** was synthesized according to GP-A from isoindoline (**10**). The crude product **13** (860 mg, 3.60 mmol, 86 %.) was obtained as a red solid and used without further purification. **^{1}H NMR** (400 MHz, $CDCl_3$) $\delta = 7.34$ (d, $J =$ 8.6 Hz, 2H), 7.18 (m, 4H), 6.90 (d, $J = 8.7$ Hz, 2H), 3.92 (s, 4H), 3.86 (s, 2H), 3.82 (s, 3H) ppm. **^{13}C NMR** (101 MHz, $CDCl_3$) $\delta = 158.9$, 140.4, 131.4, 130.1, 126.8, 122.5, 113.9, 59.8, 59.0, 55.4 ppm. **ESI-MS:** *m/z* calculated for $[M+H]^+$: 437.06, found: 437.05. **mp** = 75 °C.

4.1.2.3. 2-(4-Methoxybenzyl)-5-phenylisoindoline (14). Compound **14** was synthesized according to GP-B from **12** and 4,4,5,5-tetramethyl-2-phenyl-1,3,2-dioxaborolane. The product **14** (373 mg, 1.18 mmol, 75 %) was obtained as a brown solid after purification by column chromatography (PE/EtOAc 10:1–5:1). **^{1}H NMR** (400 MHz, $CDCl_3$) $\delta =$ 7.56 (d, $J = 8.6$ Hz, 2H), 7.45–7.40 (m, 4H), 7.38–7.31 (m, 3H), 7.25 (d, $J = 8.5$ Hz, 1H), 6.91 (d, $J = 8.6$ Hz, 2H), 3.98 (s, 2H), 3.96 (s, 2H), 3.89 (s, 2H), 3.83 (s, 3H) ppm. **^{13}C NMR** (101 MHz, $CDCl_3$) $\delta = 158.9$, 141.6, 141.2, 140.3, 139.6, 131.4, 130.1, 128.8, 127.3, 127.2, 126.0, 122.7, 121.3, 113.9, 59.8, 59.0, 58.7, 55.4 ppm. **ESI-MS:** *m/z* calculated for $[M+H]^+$: 316.16, found: 316.20. **mp** = 134 °C.

4.1.2.4. 5-Benzyl-2-(4-methoxybenzyl)isoindoline (15). Compound **15** was synthesized according to GP-B from **12** and 2-benzyl-4,4,5,5-tetramethyl-1,3,2-dioxaborolane. The product **15** (360 mg, 1.09 mmol, 70 %) was obtained as a brown oil after purification by column chromatography (PE:EtOAc 10:1–5:1). **^{1}H NMR** (400 MHz, $CDCl_3$) $\delta = 7.32$ (d, $J =$ 8.7 Hz, 2H), 7.31–7.26 (m, 2H), 7.23–7.13 (m, 4H), 7.09 (d, $J = 7.5$ Hz, 1H), 7.04–6.99 (m, 1H), 6.89 (d, $J = 8.7$ Hz, 2H), 3.94 (s, 2H), 3.87 (s, 3H), 3.84 (s, 2H), 3.82 (s, 2H), 3.80 (s, 2H) ppm. **^{13}C NMR** (101 MHz, $CDCl_3$) $\delta = 158.9$, 141.5, 140.7, 139.8, 138.2, 131.3, 130.0, 129.0, 128.5, 127.6, 126.1, 123.1, 122.4, 113.9, 59.7, 58.9, 58.7, 55.4, 41.9 ppm. **ESI-MS:** *m/z* calculated for $[M+H]^+$: 330.18, found: 330.20.

4.1.2.5. 4-(Isoindolin-2-ylmethyl)phenol (7a). Compound **7a** was synthesized according to GP-C from **13**. The product **7a** (315 mg, 1.40 mmol, 79 %) was obtained as a colorless solid and converted without further purification. For the Ellman's assay a small amount of the crude was purified by flash column chromatography (H_2O/MeCN 5-15-95 % + 0.1 % FA). **^{1}H NMR** (400 MHz, MeOD) $\delta = 8.41$ (s, 1H), 7.36–7.35 (m, 4H), 7.33 (d, $J = 8.6$ Hz, 2H), 6.87 (d, $J = 8.6$ Hz, 2H), 4.47 (s, 4H), 4.34 (s, 2H) ppm. **^{13}C NMR** (101 MHz, MeOD) $\delta = 160.3$, 135.3, 133.0, 130.1, 124.0, 122.7, 117.1, 59.1 ppm. **ESI-MS:** *m/z* calculated for [M+H]+: 226.12, found: 226.15. **mp** = 119 °C.

4.1.2.6. 4-((5-Phenylisoindolin-2-yl)methyl)phenol (8a). Compound **8a** was synthesized according to GP-C from **14**. The product **8a** (278 mg, 0.92 mmol, 83 %) was obtained as a green solid and used without further purification. **^{1}H NMR** (400 MHz, $CDCl_3$) $\delta = 8.58$ (s, 1H), 7.56–7.51 (m, 3H), 7.47–7.40 (m, 3H), 7.39–7.35 (m, 1H), 7.33–7.30 (m, 2H), 7.29–7.27 (m, 1H), 6.82 (d, $J = 7.8$ Hz, 2H), 4.50 (s, 2H), 4.48 (s, 2H), 4.20 (s, 2H) ppm. **^{13}C NMR** (101 MHz, $CDCl_3$) $\delta = 168.6$, 159.1, 142.4, 140.3, 135.2, 133.4, 131.9, 129.1, 128.0, 127.9, 127.3, 123.5, 121.8, 121.5, 116.5, 58.8, 57.3, 57.1 ppm. **ESI-MS:** *m/z* calculated for $[M+H]^+$: 302.39, found: 302.15. **mp** = 121 °C.

4.1.2.7. 4-((5-Benzylisoindolin-2-yl)methyl)phenol (9a). Compound **9a** was synthesized according to GP-C from **15**. The product **9a** (269 mg, 0.85 mmol, 74 %) was obtained as a brown oil and used without further purification. **^{1}H NMR** (400 MHz, $CDCl_3$) $\delta = 8.57$ (s, 1H), 7.31–7.27 (m, 2H), 7.24–7.20 (m, 2H), 7.19–7.13 (m, 5H), 7.04 (s, 1H), 6.78 (d, $J =$ 8.2 Hz, 2H), 4.36–4.32 (m, 4H), 4.11 (s, 2H), 3.96 (s, 2H) ppm. **^{13}C NMR** (101 MHz, $CDCl_3$) $\delta = 168.4$, 159.1, 142.6, 140.4, 134.5, 131.9, 129.7, 129.1, 128.8, 126.5, 123.6, 123.2, 121.1, 116.5, 58.8, 57.3, 57.1, 41.8 ppm. **ESI-MS:** *m/z* calculated for $[M+H]^+$: 316.16, found: 316.20.

4.1.2.8. 4-(Isoindolin-2-ylmethyl)phenyl (2,2,2,2-tetramethyl-2λ^6-propyl) carbamate (7b). Compound **7b** was synthesized according to GP-D from **7a**. The product **7b** (110 mg, 0.30 mmol, 45 %) was obtained as a colorless oil after purification by flash column chromatography (H_2O/MeCN 5-20-40-95 % + 0.1 % FA). **^{1}H NMR** (400 MHz, $CDCl_3$) $\delta = 7.39$ (d, $J = 8.4$ Hz, 2H), 7.18 (m, 4H), 7.11 (d, $J = 8.5$ Hz, 2H), 5.03 (t, $J =$ 5.7 Hz, 1H), 3.94 (s, 4H), 3.90 (s, 2H), 3.26 (q, $J = 7.0$ Hz, 2H), 1.57 (p, $J = 7.2$ Hz, 2H), 1.37–1.26 (m, 8H), 0.90 (t, $J = 6.9$ Hz, 3H) ppm. **^{13}C NMR** (101 MHz, $CDCl_3$) $\delta = 154.8$, 150.4, 140.2, 136.0, 129.7, 126.9, 122.5, 121.6, 59.7, 59.0, 41.4, 31.9, 30.0, 29.1, 26.9, 22.7, 14.2 ppm. **ESI-MS:** *m/z* calculated for $[M+H]^+$: 367.23, found: 367.25.

4.1.2.9. 4-((5-Phenylisoindolin-2-yl)methyl)phenyl (2,2,2,2-tetramethyl-2λ^6-propyl)carbamate (8b). Compound **8b** was synthesized according to GP-D from **8a**. The product **8b** (29 mg, 0.06 mmol, 20 %) was obtained as a brown solid after purification by flash column chromatography (H_2O/MeCN 0-15-95 % + 0.1 % FA). **^{1}H NMR** (400 MHz, $CDCl_3$) $\delta =$ 7.60 (d, $J = 8.4$ Hz, 2H), 7.48–7.42 (m, 6H), 7.39–7.34 (m, 1H), 7.30–7.26 (m, 1H), 7.16 (d, $J = 8.4$ Hz, 2H), 5.16 (t, $J = 5.4$ Hz, 1H), 4.02 (s, 2H), 4.00 (s, 2H), 3.95 (s, 2H), 3.28 (q, $J = 6.8$ Hz, 4H), 1.59 (p, $J = 6.7$ Hz, 2H), 1.43–1.29 (m, 8H), 0.94 (t, $J = 6.8$ Hz, 3H) ppm. **^{13}C NMR** (101 MHz, $CDCl_3$) $\delta = 154.8$, 150.3, 141.5, 141.1, 140.3, 139.5, 136.1, 129.6, 128.8, 127.3, 127.2, 126.0, 122.7, 121.6, 121.3, 59.8, 59.0, 58.8, 41.4, 31.8, 29.9, 29.0, 26.8, 22.7, 14.2 ppm. **ESI-MS:** *m/z* calculated for $[M+H]^+$: 443.60, found: 443.25. **mp** = 117 °C.

4.1.2.10. 4-((5-Benzylisoindolin-2-yl)methyl)phenyl (2,2,2,2-tetramethyl-2λ^6-propyl)carbamate (9b). Compound **9b** was synthesized according to GP-D from **9a**. The product **9b** (33 mg, 0.07 mmol, 23 %) was obtained as a beige oil after purification by flash column chromatography (H_2O/MeCN 0-35-95 % + 0.1 % FA). **^{1}H NMR** (400 MHz, $CDCl_3$) $\delta = 7.40$ (d, $J =$ 8.2 Hz, 2H), 7.30–7.24 (m, 2H), 7.21–7.14 (m, 3H), 7.12–7.07 (m, 3H), 7.05–6.99 (m, 2H), 5.03 (t, $J = 5.9$ Hz, 1H), 3.95 (s, 2H), 3.93 (s, 4H), 3.91 (s, 2H), 3.26 (q, $J = 6.7$ Hz, 2H), 1.57 (p, $J = 7.1$ Hz, 2H), 1.39–1.26 (m, 8H), 0.90 (t, $J = 6.9$ Hz, 2H) ppm. **^{13}C NMR** (101 MHz, $CDCl_3$) $\delta = 154.7$, 150.4, 141.4, 140.2, 140.1, 137.6, 135.5, 129.9, 129.0, 128.6, 127.8, 126.2, 123.1, 122.5, 121.7, 59.6, 58.9, 58.6, 41.9, 41.4, 31.9, 30.0, 29.1, 26.9, 22.7, 14.2 ppm. **ESI-MS:** *m/z* calculated for $[M+H]^+$: 457.28, found: 457.25.

4.1.2.11. 4-(Isoindolin-2-ylmethyl)phenyl azetidine-1-carboxylate (7c). Compound **7c** was synthesized according to GP-E from **7a**. The product **7c** (90 mg, 0.29 mmol, 33 %) was obtained as a colorless oil after purification by flash chromatography (H_2O/MeCN 5-20-40-95 % + 0.1 % FA). **^{1}H NMR** (400 MHz, $CDCl_3$) $\delta = 7.39$ (d, $J = 8.5$ Hz, 2H), 7.18 (m, 4H), 7.10 (d, $J = 8.6$ Hz, 2H), 4.27–4.06 (m, 4H), 3.93 (s, 4H),

3.89 (s, 2H), 2.33 (p, $J = 7.7$ Hz, 2H) ppm. **^{13}C NMR** (101 MHz, $CDCl_3$) δ = 154.5, 150.3, 140.3, 136.1, 129.7, 126.8, 122.5, 121.6, 59.8, 59.1, 50.4, 49.3, 15.9 ppm. **ESI-MS:** *m/z* calculated for $[M+H]^+$: 309.15, found: 309.15.

4.1.2.12. 4-((5-Phenylisoindolin-2-yl)methyl)phenyl azetidine-1-carboxylate (8c). Compound **8c** was synthesized according to GP-E from **8a**. The product **8c** (29 mg, 0.075 mmol, 23 %) was obtained as a colorless solid after purification by flash column chromatography (H_2O/MeCN 0-25-95 % + 0.1 % FA). **^{1}H NMR** (400 MHz, $CDCl_3$) $\delta = 7.56$ (d, $J = 7.8$ Hz, 2H), 7.46–7.39 (m, 6H), 7.36–7.31 (m, 1H), 7.24 (s, 1H), 7.12 (d, $J = 8.5$ Hz, 2H), 4.27–4.08 (m, 4H), 4.02 (s, 2H), 4.00 (s, 2H), 3.94 (s, 2H), 2.33 (p, $J = 7.7$ Hz, 2H) ppm. **^{13}C NMR** (101 MHz, $CDCl_3$) δ = 154.4, 150.4, 141.5, 140.7, 140.4, 139.1, 135.6, 129.8, 128.8, 127.3, 127.2, 126.1, 122.8, 121.6, 121.3, 59.7, 58.9, 58.7, 50.4, 49.3, 15.9 ppm. **ESI-MS:** *m/z* calculated for $[M+H]^+$: 385.18, found: 385.20. **mp** = 115 °C.

4.1.2.13. 4-((5-Benzylisoindolin-2-yl)methyl)phenyl azetidine-1-carboxylate (9c). Compound **9c** was synthesized according to GP-E from **9a**. The product **9c** (26 mg, 0.7 mmol, 21 %) was obtained as a beige oil after purification by flash column chromatography (H_2O/MeCN 0-30-95 % + 0.1 % FA). **^{1}H NMR** (400 MHz, $CDCl_3$) $\delta = 7.40$ (d, $J = 8.4$ Hz, 2H), 7.30–7.27 (m, 1H), 7.26–7.24 (m, 1H), 7.21–7.13 (m, 3H), 7.10 (d, J = 8.6 Hz, 3H), 7.05–6.99 (m, 2H), 4.28–4.05 (m, 4H), 3.98 (s, 4H), 3.95 (s, $J = 3.3$ Hz, 2H), 3.94 (s, 2H), 2.33 (p, $J = 8.0$ Hz, 2H) ppm. **^{13}C NMR** (101 MHz, $CDCl_3$) δ = 154.5, 150.7, 141.4, 140.4, 139.8, 137.2, 130.1, 129.1, 128.7, 128.1, 126.3, 123.3, 122.6, 121.8, 59.6, 58.8, 58.6, 50.5, 49.5, 42.0, 16.0 ppm. **ESI-MS:** *m/z* calculated for $[M+H]^+$: 399.20, found: 399.20.

4.1.2.14. 4-Nitrophenyl azetidine-1-carboxylate. Azetidine (271 µL, 230 mg, 4.03 mmol, 1.0 eq.) was dissolved in CH_2Cl_2 (52 mL). Nitrophenylchloroformate (893 mg, 4.43 mmol, 1.1 eq.) and Et_3N (1.6 mL, 1.22 mg, 12.1 mmol, 3.0 eq.) were added and the reaction mixture was stirred at for 16 h. The reaction was terminated by the addition of citric acid (100 mL) and the organic layer was diluted with CH_2Cl_2 (100 mL). The organic layer was washed with citric acid (2 x 50 mL) and brine (50 mL). The combined organic layers were washed with brine, dried over Na_2SO_4, filtered and the solvent was removed under reduced pressure. 4-Nitrophenyl azetidine-1-carboxylate (710 mg, 3.20 mmol, 79 %) was obtained as a colorless solid after purification by column chromatography (PE:EtOAc 5:2). **^{1}H NMR** (400 MHz, $CDCl_3$) $\delta = 8.22$ (d, J = 9.2 Hz, 2H), 7.30 (d, $J = 9.2$ Hz, 2H), 4.19 (d, $J = 41.9$ Hz, 4H), 2.36 (d, $J = 7.4$ Hz, 2H) ppm. **ESI-MS:** *m/z* calculated for $[M+H]^+$: 223.06, found: 223.10 [53].

4.2. ChE inhibition

Experiments on ChEs were performed as reported in our previous publications [27,53,60]. *h*BChE (E.C. 3.1.1.8, from humans) was kindly provided by Oksana Lockridge from the University of Nebraska Medical Center. *h*AChE, Acetylthiocholiniodid (ATC), Butyrylthiocholiniodid (BTC), bovine serum albumin (BSA) and 5,5′-Dithiobis(2-nitrobenzoic acid) (DTNB) were obtained from Sigma-Aldrich (St. Louis, Missouri). Phosphate buffer (buffer A) was prepared by dissolving NaH_2PO_4 in water (55 mM) and adjusting a pH 8.0 by addition of NaOH (0.1 M). A second buffer (buffer B) was prepared by dissolving DNTB in buffer A (0.3 mM). ATC and BTC solutions (75 mM and 45 mM) were prepared with water. Enzyme stock solutions (1.76 µg/mL) were prepared by dilution with buffer A and addition of 1 mg/mL BSA. Compounds stock solutions were prepared in DMSO (4 mM) All experiments were carried out at 25 °C and as triplicates.[27]

IC_{50} determination. Test compound stock solutions were diluted with buffer A to a starting concentration of 10 µM or 100 µM according to the compound's activity. Further dilutions were prepared with buffer B on a 96-well plate (>1 % DMSO) to obtain twelve different concentrations with a volume of 130 µL in each well. Negative control was performed in each plate using buffer A instead of compound solution and perform dilutions with buffer B as for compounds. 10 µL of the respective enzyme solution (1.76 µg/mL) were added and incubated for 20 min. Then 3 µL of the respective substrate solution (ATC or BTC, 75 mM) were added rapidly with a dispenser and enzyme activity was measured immediately by UV absorption ($\lambda = 412$ nm). Read out was carried out every 30 s over 3 min (Spectramax 190 microplate reader, Molecular Devices, San José, California). The respective enzyme activity for each concentration was calculated via the slope of all 7 measurement points. Enzyme activity was blotted against the logarithmic compound concentration and IC_{50} values were calculated by Graphpad using a sigmoidal fit and presented as means ± SEM.[27]

4.2.1. Carbamylation

To determine the on-kinetic, the experimental setup for determining the IC_{50} values was replicated, with the incubation time of the enzyme varying (5 min, 10 min, 15 min, 40 min and 60 min).[27]

4.2.2. Decarbamylation

To determine the off-kinetic, compounds were diluted in buffer and 30 µL *h*BChE stock solution (2.2 µg/mL) to a final volume of 200 µL (1000-fold concentration of the respective IC_{50} value for enzyme inhibition >85 %). For the negative control, buffer A and the respective percentage of DMSO was used instead of compound stock solution. After 1 h of incubation, 2 µL of each compound solution were rapidly added to 2 mL of buffer B (0.9 mM DTNB) by dispenser. The obtained solutions were transferred to a 96-well plate and 2 µL BTC (45 mM) was added at one row for each of eight different time points. Read outs were performed as described above for IC_{50} determination. Enzyme activity was blotted against the time after dilution to determine the half-life time of inhibition.[27]

4.3. S1R radioligand binding

Haloperidol (4-[4-(4-Chlorophenyl)-4-hydroxy-1-piperidyl]-1-(4-fluorophenyl)-butan-1-one) was purchased from Alfa Aesar (Karlsruhe, Germany). [^{3}H](+)-pentazocine was purchased from Biotrend Chemikalien GmbH (Köln, Germany).

4.3.1. Membrane preparation

Male Wistar rats (ENVIGO, UK) were decapitated, and their livers were dissected and removed to ice-cold 10 mM Tris-HCl, pH 7.4, containing 0.32 M sucrose. Livers were homogenized (after mincing with scissors) using a Potter-Elvehjem Teflon-glass homogenizer in 10 mL/g tissue wet weight of ice-cold 10 mM Tris-HCl/0.32 M sucrose, pH 7.4. The crude homogenate was centrifuged for 10 min at 1000 *g* and the pellets were discarded. The resultant supernatant was centrifuged at 31,000 *g* for 15 min. The pellet was resuspended in 3 mL/g 10 mM Tris-HCl, pH 7.4 by vortexing, and the suspension was allowed to incubate at 25 °C for 15 min. Following centrifugation at 31000×*g* for 15 min, the pellet was resuspended to 1.53 mL/g in 10 mM Tris-HCl, pH 7.4 by gentle Potter-Elvehjem homogenization and aliquots stored at −80 °C until use. Protein concentration was determined by the method of Lowry *et al.* [63] using bovine serum albumin as standard.

4.3.2. [^{3}H](+)-pentazocine binding assay

The binding assay buffer consisted of 60 µL of incubation buffer (50 mM tris(hydroxymethyl)aminomethane (TRIS)-HCl, pH = 8.0, 25 °C), 100 µL of membrane aliquots, 20 µL of the tested substances, or incubation buffer for the control, and 20 µL of [^{3}H](+)-pentazocine. The final concentration of [^{3}H](+)-pentazocine was 1.2 nM. All compounds were dissolved in dimethyl sulfoxide at a concentration of 10 mM as stock solutions. These stock solutions were diluted with 100 % DMSO at a concentration of 1 mM and following dilutions with 10 % DMSO TRIS-

HCl at 50 mM to the required concentrations. Nonspecific binding was assessed by adding haloperidol (10 μM). The radioligand and tested compounds were added to the membranes and were then incubated for 150 min at 37 °C in dark conditions using a Thermo-Shaker (BioSan, PST-60HL-4). The bound and free radioligands were separated by rapid filtration under vacuum using Millipore GF/C filter paper (Merck Millipore, Billerica, Massachusetts, USA) pre-soaked with 0.5 % polyethylenimine in 10 mM TRIS-HCl, pH 7.4, for at least 1 h before use. The filters were washed four times with 0.25 mL of 10 mM TRIS-HCl (pH 8.0, 4 °C). The radioactivity of the samples was measured with a liquid scintillation microplate counter MicroBeta2 (PerkinElmer, Waltham, Massachusetts, USA) with 30 % efficiency. Each experiment was repeated at least three times, and each assay was conducted in duplicate [64,65].

4.4. S1R–BiP dissociation

Green fluorescent protein (GFP)-tagged S1R protein-overexpressing CHO cells (gift from Drs Yuko Yasui and Tsung-Ping Su, NIDA/NIH, Baltimore, MD, USA), were expanded in minimum essential medium culture medium supplemented with 10 % heat-inactivated fetal bovine serum and 2 mmol/L Glutamax (Invitrogen, Carlsbad, CA, USA). After plating the cells, different concentrations of each compound were added for 30 min (37 °C) and the culture medium was replaced by phosphate buffered saline (3 mL). The cells were harvested and suspended in 50 mmol/L Hepes pH 7.4, then cross-linked with 50 μg/mL of dithiobissuccinimidyl propionate (Thermoscientific, Waltham, MA, USA). The reaction was terminated by adding Tris/HCl 50 mmol/L pH 8.8. After incubating 15 min on ice, the cells were lysed in 50 mmol/L Tris pH 7.4 buffer, containing 150 mmol/L NaCl, 1 % Triton X-100, 0.3 % sodium deoxycholate, 0.1 % sodium dodecylsulfate, and protease inhibitor cocktail (Roche Applied Science, Basel, Switzerland). After centrifugation at 16,000×*g* for 1 min, the supernatant was incubated with Chromotek GFP-trap agarose (Proteintech, United Kingdom) overnight at 4 °C. After centrifugation at 16,000×*g* for 1 min, the supernatant was discarded and the pellet was suspended in 0.5 mL buffer (50 mmol/L Tris (pH 7.4), 150 mmol/L NaCl, 1 % Triton X/100, 0.3 % sodium deoxycholate, 0.1 % SDS), rinsed twice, and analyzed by Heat Shock 70 KDa Protein 5 ELISA assay (#CL-SEC343Mu, Euromedex, Souffelweyersheim, France) [68].

4.5. Computational studies

Ligand structures were built in Molecular Operating Environment (MOE version 2024.0601, Chemical Computing Group, Canada) and energy-minimized with the MMFF94x force field [85] to a root-mean-square (rms) gradient of 0.001 kcal/(mol Å). The isoindoline was protonated at the tertiary amine leading to formally chiral ligands for **8a**, **8b**, **8c**, **9a**, **9b** and **9c**, which were modeled in both enantiomeric forms.

Covalent docking studies to *h*BChE and *h*AChE were performed using Glide v10.1 with Covalent Docking v1.3 in Pose Prediction Mode [76] of Schrödinger Release 2023-4 (CovDock, Schrödinger, LLC, New York, NY, 2023). The crystal structure 4M0E [86] for AChE (resolution 2.00 Å) and 6QAA [87] for BChE (resolution 1.90 Å), which has been used in our previous work [26,72], was employed. All water and non-protein molecules were removed and hydrogens were added to the protein residues with MOE at pH = 7. The catalytic histidine (His447 for AChE and His438 for BChE) was maintained in its protonated state, as the following covalent docking aims to model the covalent tetrahedral intermediate. The grid was generated on the run during docking and was centered at the centroid of the reactive Ser203 and Phe338 for AChE, which corresponds to Ser198 and Phe329 in BChE. A box size of 15 Å for the inner and 40 Å for the outer box was selected. Constraints were applied and had to be satisfied by at least one hydrogen bond between the carbonyl-oxygen of the ligand and the backbone-nitrogen of the glycines that form the oxyanion hole. As reaction type a custom reaction ("index 6") was obtained from Schrödinger's covalent reactions repository [88]. A maximum of ten poses per ligand were generated. Poses were ranked by their Prime Energy. For geometry optimization, a short energy minimization of the ligand was performed using the OPLS_2005 force field. The two top-ranked poses were visually analyzed and the preferred one selected by interaction patterns. The representative enantiomer for the binding mode was selected by docking score, considering contributions of the non-covalent and covalent state for binding.

Non-covalent docking studies at the S1R were carried out with Glide v10.1 using standard precision (SP) with GlideScore version SP5.0 of Schrödinger release 2023-4 (Glide, Schrödinger, LLC, New York, NY. 2023). The crystal structure 5HK1 [55] with the best resolution of 2.51 Å in the Protein Database (PDB) was selected and only chain A of the homotrimer was used. Prior to docking, all water and non-protein molecules were removed and hydrogens were added to the protein residues with MOE at physiological pH (7.4). Asp126 was included in the protonated state as it interacts with Glu172 via a hydrogen bond. The grid used for docking was centered at the centroid of Val84 and Glu172, the inner box was set to a size of 10 Å and the outer box to 40 Å. By default, the OPLS_2005 force field [89] was applied. Docking was performed with enhanced conformational sampling by a factor of 3. A maximum of ten poses per ligand were generated and ranked by their GlideScore which is an empirical scoring function approximating ligand binding free energy that enables comparison to experimental results. The two top-ranked poses were visually analyzed and the preferred selected by interaction patterns. The representative enantiomer for the binding mode was selected by GlideScore and occurrence of interaction patterns with the residues of the binding site.

Validation was carried out by redocking of the crystallized ligands. The RMSD of the top-ranked pose for the redocking of PD144418 in 5HK1 was 0.860 Å; for Dihydrotanshinone I in 4M0E an RMSD of 0.424 Å and for (S)-2-(butylamino)-N-(2-cycloheptylethyl)-3-(1H-indol-3-yl)propanamide in 6QAA (including the crystallized and interacting DMSO molecule in the binding site) an RMSD of 0.637 Å was obtained.

All figures of docking poses were generated with PyMol (The PyMOL Molecular Graphics System, version 2.6.1; Schrödinger, LLC).

4.6. Neurotoxicity

HT22 cells were grown in Dulbecco's modified Eagle medium (Sigma Aldrich, St. Louis, Missouri) supplemented with 10 % (v/v) fetal calf serum and 1 % (v/v) penicillin– streptomycin. Cells were subcultured every two days and incubated at 37 °C with 5 % CO_2 in a humidified incubator. Compounds were dissolved in DMSO (Sigma Aldrich, Munich, Germany) as stock solutions and diluted further into culture medium. For determination of cell viability, a colorimetric 3-(4,5-dimethylthiazol-2-yl)-2,5-diphenyl tetrazolium bromide (MTT, Sigma Aldrich, Munich, Germany) assay was used. MTT solution (4 mg/mL in PBS) was diluted 1:10 with medium and added to the wells after removal of the old medium. Cells were incubated for 3 h and then lysis buffer (10 % SDS) was applied. The next day, absorbance at 560 nm was determined with a multiwell plate photometer (Tecan, SpectraMax 250) [27,53]. For the neurotoxicity assay, $5x10^3$ cells per well were seeded into sterile 96-well plates and incubated overnight. The next day, medium was removed and the compound, diluted from a 10 mM stock solution into the indicated concentrations using fresh medium, was added to the wells. 0.05 % DMSO in Dulbecco's modified Eagle medium served as a control. Cells were incubated for 24 h when neurotoxicity was determined using a colorimetric MTT assay. Measurements were performed in three independent experiments.

4.7. Solubility

For solubility measurements, a 10 mg/mL stock solution in DMSO

was prepared for each HCl salt. A dilution row with concentrations of 100, 80, 40, 20 and 10 μg/mL in MeOH were prepared for the calibration curve. The dilutions were measured via HPLC using the method described in the general information. The UV peak areas were plotted against the concentration to give the calibration curve. For solubility determination, 8 μL of sample stock solution was added into 792 μL PBS and shaken overnight. After centrifugation (2000 g, 2 min) and filtration, the samples were analyzed by HPLC.[27,79] Measurements were performed in three independent experiments.

4.8. *In vivo studies in the $A\beta_{25-35}$ mouse model*

Mice were treated IP with the compounds dissolved in 10 % DMSO in saline, once-a-day between day 1 and day 7. On day 8, the short-term memory of the mice was tested using spontaneous alternation in the Y-maze. Effects on long-term memory were assessed on day 9 (training) and day 10 (test) using the step-through type passive avoidance test.[27,28,90,91]

4.8.1. *Animals*

Male Swiss-OF1 mice, 7 weeks old, weighing 32 ± 5 g, were supplied from JANVIER labs (Saint Berthevin, France). Homozygous BuChE KO founders were provided by Dr. O. Lockridge (Eppley Institute, University of Nebraska Medical Center, Omaha,NE, USA).[92] The colony was then maintained on a pure 129/Sv strain at the animal facility of INRAE in Montpellier (agreement no. D34-172-10). WT and homozygous (KO) littermates were transferred to the animal facility building of the University of Montpellier (CECEMA, Office of Veterinary Services agreement # B-34-172-23) at least 1 week before the behavioral experiments start. Upon arrival, animals were divided into groups and housed with access to food and water *ad libitum* except during behavioral tests. Mice were kept in a temperature- and humidity-controlled animal facility on a 12 h/12 h light/dark cycle (lights off at 07:00 p.m.). Behavioral experiments were conducted between 8:00 a.m. and 5:00 p.m. in a sound-attenuated and air-regulated experimental room. All animal procedures were conducted in strict adherence to the European Union directive of September 22, 2010 (2010/63/UE) and the ARRIVE guidelines. The project was authorized by the French National Ethic Committee (APAFIS no. #37113–2022050615297921) [28].

4.8.2. *Preparation and administration of injection solutions*

The $A\beta_{25-35}$ peptide was solubilized at 3 μM in water (vehicle solution, V) and oligomerized by incubation at 37 °C for 4 days. Mice were anesthetized with 2.5 % isoflurane and injected ICV with $A\beta_{25-35}$ (9 nmol in 3 μL). Compounds were dissolved in 100 % DMSO at a concentration of 6 mg/mL, further diluted with physiological saline (0.9 % NaCl) to a final percentage of 10 % DMSO and injected IP. The vehicle solution was prepared with 10 % DMSO in physiological saline and injected IP. After all injections, the behavior of the mice in their home cage was checked visually [28].

4.8.3. Behavioral tests. At day 7 after injection, animals were tested in the Y-maze for their spontaneous alternation behavior, an index of spatial working memory. At days 8 and 9, a passive avoidance test was performed to measure the non-spatial long-term memory, as described previously [53].

CRediT authorship contribution statement

Kora Reichau: Writing – original draft, Visualization, Investigation, Formal analysis, Data curation. **Lucie Crouzier:** Investigation, Formal analysis, Data curation. **Tina Gehrig:** Writing – review & editing, Software, Investigation, Data curation. **Alix Flake:** Writing – review & editing, Investigation, Formal analysis. **Eva Schaller:** Investigation, Data curation. **Johann Meunier:** Validation, Investigation, Data curation. **Christelle Bertrand-Gaday:** Methodology, Data curation. **Arnaud Chatonnet:** Supervision, Resources. **Liga Zvejniece:** Writing – review & editing, Resources, Project administration, Investigation, Funding acquisition, Data curation. **Christoph Sotriffer:** Writing – review & editing, Supervision, Methodology. **Tangui Maurice:** Writing – review & editing, Visualization, Supervision, Resources, Project administration, Funding acquisition, Formal analysis, Data curation, Conceptualization. **Michael Decker:** Writing – review & editing, Supervision, Resources, Project administration, Methodology, Funding acquisition, Formal analysis, Conceptualization.

Funding sources

M.D. and T.M. acknowledge a bi-national funding from the Deutsche Forschungsgemeinschaft (DFG) and French Agence National de la Recherche (ANR) through a cooperative DFG/ANR grant (project DFG DE1546/12-1, ANR-22-CE92-0080). Campus France (PHC Procope), BayFrance (Franco-Bavarian University cooperation, FK03-2020) and the German Academic Exchange Service (DAAD, Deutscher Akademischer Austauschdienst, 57702280) are gratefully acknowledged for funding travel costs. The work has been supported through the European Cooperation in Science and Technology (COST Association), SIGMA1_EUROPE action under No. CA23156 and by RRF grant No.53/OSI/PA (RRF project No.5.2.1.1.i.0/2/24/I/CFLA/001).

Declaration of competing interest

The authors declare no competing interests.

Acknowledgement

*h*BChE was kindly donated by Dr. O. Lockridge (University of Nebraska Medical Center). S1R-overexpressing CHO cells were kindly provided by Dr. Y. Yasui and Dr. T.P. Su (NIDA/NIH, Baltimore, MD, USA). We thank the INRAE SupAgro and CECEMA-UM animal facilities for animal housing and experiments. The TOC graphic was created in BioRender. Decker, M. (2025) https://BioRender.com/uta791g.

Glossary

ACh	Acetylcholine
ATC	Acetylthiocholine
AD	Alzheimer's Disease
Aβ	Amyloid Beta
ANOVA	Analysis of Variance
BiP	Binding Immunoglobulin Protein
BDNF	brain-derived neurotrophic factor
BSA	Bovine Serum Albumin
BTC	Butyrylcholinesterase
CHO	Chinese Hamster Ovary
ChE	Cholinesterase
CI	Combination Index
DMSO	Dimethyl Sulfoxide
DMF	Dimethylformamide
MTT	3-(4,5-Dimethylthiazol-2-yl)-2,5-Diphenyltetrazolium Bromide
DTNB	5,5′-Dithiobis(2-Nitrobenzoic Acid)
ESI-MS	Electrospray Ionization Mass Spectrometry
ER	Endoplasmic Reticulum
EPC	Enzyme-Phenolcarbamate Complex
GP	General Procedure
EC_{50}	Half Maximal Effective Concentration
IC_{50}	Half Maximal Inhibitory Concentration
HPLC	High-Performance Liquid Chromatography
HT22	Murine Hippocampal Neuronal Cell Line
*h*AChE	Human Acetylcholinesterase
*h*BChE	Human Butyrylcholinesterase
IP_3R	Inositol 1,4,5-Trisphosphate Receptor

ICV	Intracerebroventricular
IP	Intraperitoneal
KO	Knockout
LCMS	Liquid Chromatography-Mass Spectrometry
NFTs	Neurofibrillary Tangles
NMR	Nuclear Magnetic Resonance
PBS	Phosphate-Buffered Saline
ROS	Reactive Oxygen Species
SI	Selectivity Index
S1R	Sigma-1 Receptor
SEM	Standard Error of the Mean
THF	Tetrahydrofuran
TRIS	Tris(hydroxymethyl)aminomethane
UV	Ultraviolet
WT	Wild Type.

Appendix B. Supplementary data

Supplementary data to this article can be found online at https://doi.org/10.1016/j.ejmech.2025.118486.

Data availability

Data will be made available on request.

References

[1] R.A. Stelzmann, H. Norman Schnitzlein, F. Reed Murtagh, An english translation of alzheimer's 1907 paper, "über eine eigenartige erkankung der hirnrinde, Clin. Anat. 8 (1995) 429–431.

[2] M.W. Bondi, E.C. Edmonds, D.P. Salmon, Alzheimer's Disease: Past, Present, and Future, J. Int. Neuropsychol. Soc. 23 (2017) 818–831.

[3] B. Singh, C.M. Day, S. Abdella, S. Garg, Alzheimer's disease current therapies, novel drug delivery systems and future directions for better disease management, J. Control. Release. 367 (2024) 402–424.

[4] J. Stevenson-Hoare, A.-K. Schalkamp, C. Sandor, J. Hardy, V. Escott-Price, New cases of dementia are rising in elderly populations in Wales, UK, J. Neurol. Sci. 451 (2023) 120715.

[5] A.Y. Kim, S. Al Jerdi, R. MacDonald, C.R. Triggle, Alzheimer's disease and its treatment–yesterday, today, and tomorrow, Front. Pharmacol. 15 (2024) 1–30.

[6] Cathy Greenblat, Dementia, 2025. https://www.who.int/news-room/fact-sheets/detail/dementia#:~:text=In%202021%2C%2057%20million%20people,for%20people%20living%20with%20dementia. (accessed 11 September 2025).

[7] Y. Zhang, H. Chen, R. Li, K. Sterling, W. Song, Amyloid β-based therapy for Alzheimer's disease: challenges, successes and future, Signal Transduct. Target. Ther. 8 (2023) 248.

[8] M.O. Iliyasu, S.A. Musa, S.B. Oladele, A.I. Iliya, Amyloid-beta aggregation implicates multiple pathways in Alzheimer's disease: Understanding the mechanisms, Front. Neurosci. 17 (2023) 1–10.

[9] H. Hampel, J. Hardy, K. Blennow, C. Chen, G. Perry, S.H. Kim, V.L. Villemagne, P. Aisen, M. Vendruscolo, T. Iwatsubo, C.L. Masters, M. Cho, L. Lannfelt, J. L. Cummings, A. Vergallo, The Amyloid-β Pathway in Alzheimer's Disease, Mol. Psychiatry 26 (2021) 5481–5503.

[10] J.W. Kinney, S.M. Bemiller, A.S. Murtishaw, A.M. Leisgang, A.M. Salazar, B. T. Lamb, Inflammation as a central mechanism in Alzheimer's disease, Alzheimer's Dement.: Transl. Res. Clin. Interv. 4 (2018) 575–590.

[11] J. Xie, L. van Hoecke, R.E. Vandenbroucke, The Impact of Systemic Inflammation on Alzheimer's Disease Pathology, Front. Immunol. 12 (2022) 1–18.

[12] K.A. Walker, B.N. Ficek, R. Westbrook, Understanding the Role of Systemic Inflammation in Alzheimer's Disease, ACS Chem. Neurosci. 10 (2019) 3340–3342.

[13] J. Zhang, Y. Zhang, J. Wang, Y. Xia, J. Zhang, L. Chen, Recent advances in Alzheimer's disease: mechanisms, clinical trials and new drug development strategies, Signal Transduct. Target. Ther. 9 (2024) 211.

[14] B. Turgutalp, C. Kizil, Multi-target drugs for Alzheimer's disease, Trends Pharmacol. Sci. 45 (2024) 628–638.

[15] O. Benek, J. Korabecny, O. Soukup, A Perspective on Multi-target Drugs for Alzheimer's Disease, Trends Pharmacol. Sci. 41 (2020) 434–445.

[16] C. Pathak, U.D. Kabra, A comprehensive review of multi-target directed ligands in the treatment of Alzheimer's disease, Bioorg. Chem. 144 (2024) 107152.

[17] T. Sun, T. Zhen, C.H. Harakandi, L. Wang, H. Guo, Y. Chen, H. Sun, New insights into butyrylcholinesterase: Pharmaceutical applications, selective inhibitors and multitarget-directed ligands, Eur. J. Med. Chem. 275 (2024) 116569.

[18] Sultan Darvesh, Butyrylcholinesterase as a Diagnostic and Therapeutic Target for Alzheimer's Disease, Curr. Alzheimer Res. 13 (2016) 1173–1177.

[19] G.A. Reid, S. Darvesh, Butyrylcholinesterase-knockout reduces brain deposition of fibrillar β-amyloid in an Alzheimer mouse model, Neurosci 298 (2015) 424–435.

[20] B. Mendel, H. Rudney, On the Type of Cholinesterase Present in Brain Tissue, Science 98 (1943) 201–202.

[21] Q. Li, H. Yang, Y. Chen, H. Sun, Recent progress in the identification of selective butyrylcholinesterase inhibitors for Alzheimer's disease, Eur. J. Med. Chem. 132 (2017) 294–309.

[22] W. Xie, J.A. Stribley, A. Chatonnet, P.J. Wilder, A. Rizzino, R.D. McComb, P. Taylor, S.H. Hinrichs, O. Lockridge, Postnatal developmental delay and supersensitivity to organophosphate in gene-targeted mice lacking acetylcholinesterase, J. Pharmacol. Exp. Ther. 293 (2000) 896–902.

[23] M.-M. Mesulam, A. Guillozet, P. Shaw, A. Levey, E. Duysen, O. Lockridge, Acetylcholinesterase knockouts establish central cholinergic pathways and can use butyrylcholinesterase to hydrolyze acetylcholine, Neurosci 110 (2002) 627–639.

[24] U.D. Teitsdottir, T. Darreh-Shori, S.H. Lund, M.K. Jonsdottir, J. Snaedal, P. H. Petersen, Phenotypic Displays of Cholinergic Enzymes Associate With Markers of Inflammation, Neurofibrillary Tangles, and Neurodegeneration in Pre- and Early Symptomatic Dementia Subjects, Front. Aging Neurosci. 14 (2022) 1–14.

[25] J.G. Fernández-Bolaños, Ó. López, Butyrylcholinesterase inhibitors as potential anti-Alzheimer's agents: an updated patent review (2018-present), Expert Opin, Ther. Pat. 32 (2022) 913–932.

[26] M. Hoffmann, C. Stiller, E. Endres, M. Scheiner, S. Gunesch, C. Sotriffer, T. Maurice, M. Decker, Highly Selective Butyrylcholinesterase Inhibitors with Tunable Duration of Action by Chemical Modification of Transferable Carbamate Units Exhibit Pronounced Neuroprotective Effect in an Alzheimer's Disease Mouse Model, J. Med. Chem. 62 (2019) 9116–9140.

[27] P. Spatz, T. Zimmermann, S. Steinmüller, J. Hofmann, T. Maurice, M. Decker, Novel benzimidazole-based pseudo-irreversible butyrylcholinesterase inhibitors with neuroprotective activity in an Alzheimer's disease mouse model, RSC Med. Chem. 13 (2022) 944–954.

[28] A. Carles, M. Hoffmann, M. Scheiner, L. Crouzier, C. Bertrand-Gaday, A. Chatonnet, M. Decker, T. Maurice, The selective butyrylcholinesterase inhibitor UW-MD-95 shows symptomatic and neuroprotective effects in a pharmacological mouse model of Alzheimer's disease, CNS Neurosci. Ther. 30 (2024) e14814.

[29] M. Scheiner, M. Hoffmann, F. He, E. Poeta, A. Chatonnet, B. Monti, T. Maurice, M. Decker, Selective Pseudo-irreversible Butyrylcholinesterase Inhibitors Transferring Antioxidant Moieties to the Enzyme Show Pronounced Neuroprotective Efficacy In Vitro and In Vivo in an Alzheimer's Disease Mouse Model, J. Med. Chem. 64 (2021) 9302–9320.

[30] Q. Li, Y. Chen, S. Xing, Q. Liao, B. Xiong, Y. Wang, W. Lu, S. He, F. Feng, W. Liu, Y. Chen, H. Sun, Highly Potent and Selective Butyrylcholinesterase Inhibitors for Cognitive Improvement and Neuroprotection, J. Med. Chem. 64 (2021) 6856–6876.

[31] G.F. Makhaeva, N.V. Kovaleva, N.P. Boltneva, E.V. Rudakova, S.V. Lushchekina, T. Y. Astakhova, I.V. Serkov, A.N. Proshin, E.V. Radchenko, V.A. Palyulin, J. Korabecny, O. Soukup, S.O. Bachurin, R.J. Richardson, Bis-Amiridines as Acetylcholinesterase and Butyrylcholinesterase Inhibitors: N-Functionalization Determines the Multitarget Anti-Alzheimer's Activity Profile, Molecules 27 (2022) 1060.

[32] A. Meden, D. Knez, N. Malikowska-Racia, X. Brazzolotto, F. Nachon, J. Svete, K. Sałat, U. Grošelj, S. Gobec, Structure-activity relationship study of tryptophan-based butyrylcholinesterase inhibitors, Eur. J. Med. Chem. 208 (2020) 112766.

[33] A. Meden, D. Knez, X. Brazzolotto, F. Nachon, J. Dias, J. Svete, J. Stojan, U. Grošelj, S. Gobec, From tryptophan-based amides to tertiary amines: Optimization of a butyrylcholinesterase inhibitor series, Eur. J. Med. Chem. 234 (2022) 114248.

[34] T. Maurice, N. Goguadze, Sigma-1 (σ1) Receptor in Memory and Neurodegenerative Diseases, Sigma Proteins: Evolution of the Concept of Sigma Receptors, Handbook of Experimental Pharmacology 244 (2017) 81–108.

[35] T. Maurice, Bi-phasic dose response in the preclinical and clinical developments of sigma-1 receptor ligands for the treatment of neurodegenerative disorders, Expert Opin. Drug Discov. 16 (2021) 373–389.

[36] T. Hayashi, T.-P. Su, Sigma-1 Receptor Chaperones at the ER- Mitochondrion Interface Regulate Ca^{2+} Signaling and Cell Survival, Cell 131 (2007) 596–610.

[37] T.-P. Su, T.-C. Su, Y. Nakamura, S.-Y. Tsai, The Sigma-1 Receptor as a Pluripotent Modulator in Living Systems, Trends Pharmacol. Sci. 37 (2016) 262–278.

[38] T. Hayashi, T. Maurice, T.P. Su, Ca(2+) signaling via sigma(1)-receptors: novel regulatory mechanism affecting intracellular Ca(2+) concentration, J. Pharmacol. Exp. Ther. 293 (2000) 788–798.

[39] M. Shi, F. Chen, Z. Chen, W. Yang, S. Yue, J. Zhang, X. Chen, Sigma-1 Receptor: A Potential Therapeutic Target for Traumatic Brain Injury, Front. Cell. Neurosci. (2021) 1–19.

[40] M. Pannuzzo, On the physiological/pathological link between Aβ peptide, cholesterol, calcium ions and membrane deformation: A molecular dynamics study, Biochim. Biophys. Acta - Biomembr. 1858 (2016) 1380–1389.

[41] D.A. Ryskamp, S. Korban, V. Zhemkov, N. Kraskovskaya, I. Bezprozvanny, Neuronal Sigma-1 Receptors: Signaling Functions and Protective Roles in Neurodegenerative Diseases, Front. Neurosci. (2019) 1–20.

[42] S.-Y.A. Tsai, M.J. Pokrass, N.R. Klauer, H. Nohara, T.-P. Su, Sigma-1 receptor regulates Tau phosphorylation and axon extension by shaping p35 turnover via myristic acid, Proc. Natl. Acad. Sci. 112 (2015) 6742–6747.

[43] A. Pal, D. Fontanilla, A. Gopalakrishnan, Y.-K. Chae, J.L. Markley, A.E. Ruoho, The sigma-1 receptor protects against cellular oxidative stress and activates antioxidant response elements, Eur. J. Pharmacol. 682 (2012) 12–20.

[44] N. Goguadze, E. Zhuravliova, D. Morin, D. Mikeladze, T. Maurice, Sigma-1 Receptor Agonists Induce Oxidative Stress in Mitochondria and Enhance Complex I Activity in Physiological Condition but Protect Against Pathological Oxidative Stress, Neurotox. Res. 35 (2019) 1–18.

[45] T. Siddiqui, L.K. Bhatt, Targeting Sigma-1 Receptor: A Promising Strategy in the Treatment of Parkinson's Disease, Neurochem. Res. 48 (2023) 2925–2935.

[46] A. Marrazzo, F. Caraci, E.T. Salinaro, T.-P. Su, A. Copani, G. Ronsisvalle, Neuroprotective effects of sigma-1 receptor agonists against beta-amyloid-induced toxicity, NeuroReport 16 (2005) 1223–1226.
[47] J. Meunier, J. Ieni, T. Maurice, The anti-amnesic and neuroprotective effects of donepezil against amyloid beta25-35 peptide-induced toxicity in mice involve an interaction with the sigma1 receptor, Br. J. Pharmacol. 149 (2006) 998–1012.
[48] T. Maurice, T.-P. Su, A. Privat, Sigma1 (σ1) receptor agonists and neurosteroids attenuate β25–35-amyloid peptide-induced amnesia in mice through a common mechanism, Neurosci 83 (1998) 413–428.
[49] M. Mishina, M. Ohyama, K. Ishii, S. Kitamura, Y. Kimura, K. Oda, K. Kawamura, T. Sasaki, S. Kobayashi, Y. Katayama, K. Ishiwata, Low density of sigma1 receptors in early Alzheimer's disease, Ann. Nucl. Med. 22 (2008) 151–156.
[50] V. Villard, J. Espallergues, E. Keller, A. Vamvakides, T. Maurice, Anti-amnesic and neuroprotective potentials of the mixed muscarinic receptor/sigma1 (σ1) ligand ANAVEX2-73, a novel aminotetrahydrofuran derivative, J. Psychopharmacol. 25 (2010) 1101–1117.
[51] A.N. Fallica, V. Pittalà, M.N. Modica, L. Salerno, G. Romeo, A. Marrazzo, M. A. Helal, S. Intagliata, Recent Advances in the Development of Sigma Receptor Ligands as Cytotoxic Agents: A Medicinal Chemistry Perspective, J. Med. Chem. 64 (2021) 7926–7962.
[52] T.P. Su, X.Z. Wu, E.J. Cone, K. Shukla, T.M. Gund, A.L. Dodge, D.W. Parish, Sigma compounds derived from phencyclidine: identification of PRE-084, a new, selective sigma ligand, J. Pharmacol. Exp. Ther. 259 (1991) 543–550.
[53] P. Spatz, S.A.M. Steinmüller, A. Tutov, E. Poeta, A. Morilleau, A. Carles, M. H. Deventer, J. Hofmann, C.P. Stove, B. Monti, T. Maurice, M. Decker, Dual-Acting Small Molecules: Subtype-Selective Cannabinoid Receptor 2 Agonist/Butyrylcholinesterase Inhibitor Hybrids Show Neuroprotection in an Alzheimer's Disease Mouse Model, J. Med. Chem. 66 (2023) 6414–6435.
[54] R.A. Glennon, S.Y. Ablordeppey, A.M. Ismaiel, M.B. el-Ashmawy, J.B. Fischer, K. B. Howie, Structural features important for sigma 1 receptor binding, J. Med. Chem. 37 (1994) 1214–1219.
[55] H.R. Schmidt, S. Zheng, E. Gurpinar, A. Koehl, A. Manglik, A.C. Kruse, Crystal structure of the human σ1 receptor, Nature 532 (2016) 527–530.
[56] K. Linkens, H.R. Schmidt, J.J. Sahn, A.C. Kruse, S.F. Martin, Investigating isoindoline, tetrahydroisoquinoline, and tetrahydrobenzazepine scaffolds for their sigma receptor binding properties, Eur. J. Med. Chem. 151 (2018) 557–567.
[57] F.H. Darras, B. Kling, J. Heilmann, M. Decker, Neuroprotective Tri- and Tetracyclic BChE Inhibitors Releasing Reversible Inhibitors upon Carbamate Transfer, ACS Med. Chem. Lett. 3 (2012) 914–919.
[58] H. Zhang, Y. Wang, D. Liu, J. Li, Y. Feng, Y. Lu, G. Yin, Z. Li, T. Shi, Z. Wang, Carbamate-based N-Substituted tryptamine derivatives as novel pleiotropic molecules for Alzheimer's disease, Bioorg. Chem. 125 (2022) 105844.
[59] G. Huang, B. Kling, F.H. Darras, J. Heilmann, M. Decker, Identification of a neuroprotective and selective butyrylcholinesterase inhibitor derived from the natural alkaloid evodiamine, Eur. J. Med. Chem. 81 (2014) 15–21.
[60] E. Sawatzky, S. Wehle, B. Kling, J. Wendrich, G. Bringmann, C.A. Sotriffer, J. Heilmann, M. Decker, Discovery of Highly Selective and Nanomolar Carbamate-Based Butyrylcholinesterase Inhibitors by Rational Investigation into Their Inhibition Mode, J. Med. Chem. 59 (2016) 2067–2082.
[61] P. Camps, X. Formosa, C. Galdeano, T. Gómez, D. Muñoz-Torrero, L. Ramírez, E. Viayna, E. Gómez, N. Isambert, R. Lavilla, A. Badia, M.V. Clos, M. Bartolini, F. Mancini, V. Andrisano, A. Bidon-Chanal, Ó. Huertas, T. Dafni, F.J. Luque, Tacrine-based dual binding site acetylcholinesterase inhibitors as potential disease-modifying anti-Alzheimer drug candidates, Chem. Biol. Interact. 187 (2010) 411–415.
[62] A. Romero, R. Cacabelos, M.J. Oset-Gasque, A. Samadi, J. Marco-Contelles, Novel tacrine-related drugs as potential candidates for the treatment of Alzheimer's disease, Bioorg. Med. Chem. Lett. 23 (2013) 1916–1922.
[63] O. Lowry, N. Rosebrough, A.L. Farr, R. Randall, Protein measurements with the folin phenol reagent, J. Biol. Chem. 193 (1951) 265–275.
[64] E.J. Cobos, G. Lucena, J.M. Baeyens, E. Del Pozo, Differences in the allosteric modulation by phenytoin of the binding properties of the σ1 ligands [3H](+)-pentazocine and [3H]NE-100, Synapse 59 (2006) 152–161.
[65] S.B. Hellewell, A. Bruce, G. Feinstein, J. Orringer, W. Williams, W.D. Bowen, Rat liver and kidney contain high densities of σ1 and σ2 receptors: characterization by ligand binding and photoaffinity labeling, Eur. J. Pharmacol. Mol. Pharmacol. 268 (1994) 9–18.
[66] L. Zvejniece, E. Vavers, B. Svalbe, R. Vilskersts, I. Domracheva, M. Vorona, G. Veinberg, I. Misane, I. Stonans, I. Kalvinsh, M. Dambrova, The cognition-enhancing activity of E1R, a novel positive allosteric modulator of sigma-1 receptors, Br. J. Pharmacol. 171 (2014) 761–771.
[67] L. Crouzier, J. Meunier, A. Carles, A. Morilleau, C. Vrigneau, M. Schmitt, J.-J. Bourguignon, B. Delprat, T. Maurice, Convolamine, a tropane alkaloid extracted from Convolvulus plauricalis, is a potent sigma-1 receptor-positive modulator with cognitive and neuroprotective properties, Phytother. Res. 38 (2024) 694–712.
[68] L. García-Pupo, L. Crouzier, A. Bencomo-Martínez, J. Meunier, A. Morilleau, B. Delprat, M.S. Carrazana, Roberto Menéndez Soto del Valle, T. Maurice, C. Rodríguez-Tanty, et al., Amylovis-201 is a new dual-target ligand, acting as an anti-amyloidogenic compound and a potent agonist of the σ1 chaperone protein, Acta Pharm. Sin. B. 14 (2024) 4345–4359.
[69] S. Macfarlane, T. Grimmer, K. Teo, T.J. O'Brien, M. Woodward, J. Grunfeld, A. Mander, A. Brodtmann, B.J. Brew, P. Morris, C. Short, S. Kurrle, R. Lai, S. Bharadwaj, P. Drysdale, J. Sturm, S.J. Lewis, D. Barton, C. Kalafatis, S. Sharif, R. Perry, N. Mannering, J. MacSweeney, S. Pearson, C. Evans, V. Krishna, A. Thompson, M. Munisamy, N. Bhatt, A. Asher, S. Connell, J. Lynch, S.M. Rutgers, P.L.J. Dautzenberg, N. Prins, P. Oschmann, L. Frölich, P. Tacik, O. Peters, J. Wiltfang, A. Henri-Bhargava, E. Smith, S. Pasternak, A. Frank, H. Chertkow, J. Ingram, G.-Y.R. Hsiung, R. Brittain, C. Tartaglia, S. Cohen, L.M. Villa, E. Gordon, T. Jubault, N. Guizard, A. Tucker, W.E. Kaufmann, K. Jin, W.R. Chezem, C. U. Missling, M.N. Sabbagh, Blarcamesine for the treatment of Early Alzheimer's Disease: Results from the ANAVEX2-73-AD-004 Phase IIB/III trial, J. Prev. Alzheimers. Dis. 12 (2025) 100016.
[70] L. Hosie, L.D. Sutton, D.M. Quinn, p-Nitrophenyl and cholesteryl-N-alkyl carbamates as inhibitors of cholesterol esterase, J. Biol. Chem. 262 (1987) 260–264.
[71] S.R. Feaster, K. Lee, N. Baker, D.Y. Hui, D.M. Quinn, Molecular Recognition by Cholesterol Esterase of Active Site Ligands: Structure−Reactivity Effects for Inhibition by Aryl Carbamates and Subsequent Carbamylenzyme Turnover, Biochemistry 35 (1996) 16723–16734.
[72] M. Scheiner, A. Sink, M. Hoffmann, C. Vrigneau, E. Endres, A. Carles, C. Sotriffer, T. Maurice, M. Decker, Photoswitchable Pseudoirreversible Butyrylcholinesterase Inhibitors Allow Optical Control of Inhibition in Vitro and Enable Restoration of Cognition in an Alzheimer's Disease Mouse Model upon Irradiation, J. Am. Chem. Soc. 144 (2022) 3279–3284.
[73] R.A. Copeland. Evaluation of enzyme inhibitors in drug discovery. A guide for medicinal chemists and pharmacologists, John Wiley & Sons, Inc, 2013, pp. 1–576.
[74] E. Sawatzky, E. Al-Momani, R. Kobayashi, T. Higuchi, S. Samnick, M. Decker, A Novel Way To Radiolabel Human Butyrylcholinesterase for Positron Emission Tomography through Irreversible Transfer of the Radiolabeled Moiety, ChemMedChem 11 (2016) 1540–1550.
[75] R.A. Friesner, J.L. Banks, R.B. Murphy, T.A. Halgren, J.J. Klicic, D.T. Mainz, M. P. Repasky, E.H. Knoll, M. Shelley, J.K. Perry, D.E. Shaw, P. Francis, P.S. Shenkin, Glide: a new approach for rapid, accurate docking and scoring. 1. Method and assessment of docking accuracy, J. Med. Chem. 47 (2004) 1739–1749.
[76] K. Zhu, K.W. Borrelli, J.R. Greenwood, T. Day, R. Abel, R.S. Farid, E. Harder, Docking covalent inhibitors: a parameter free approach to pose prediction and scoring, J. Chem. Inf. Model. 54 (2014) 1932–1940.
[77] Y. Zhou, S. Wang, Y. Zhang, Catalytic Reaction Mechanism of Acetylcholinesterase Determined by Born−Oppenheimer Ab Initio QM/MM Molecular Dynamics Simulations, J. Phys. Chem. B 114 (2010) 8817–8825.
[78] P. Masson, M.-T. Froment, C.F. Bartels, O. Lockridge, Asp70 in the Peripheral Anionic Site of Human Butyrylcholinesterase, Eur. J. Biochem. 235 (1996) 36–48.
[79] R.P. Austin, C. Bennion, R.V. Bonnert, L. Cheema, A.R. Cook, R.J. Cox, M.R. Ebden, A. Gaw, K. Grime, P. Meghani, D. Nicholls, C. Phillips, N. Smith, J. Steele, J. P. Stonehouse, Discovery and evaluation of a novel monocyclic series of CXCR2 antagonists, Bioorg. Med. Chem. Lett. 25 (2015) 1616–1620.
[80] A. Freyssin, A. Carles, S. Guehairia, G. Rubinstenn, T. Maurice, Fluoroethylnormemantine (FENM) shows synergistic protection in combination with a sigma-1 receptor agonist in a mouse model of Alzheimer's disease, Neuropharmacology 242 (2024) 109733.
[81] P. Martin, T. Maurice, A. Gammaitoni, G. Farfel, B. Boyd, B. Galer, Fenfluramine modulates the anti-amnesic effects induced by sigma-1 receptor agonists and neuro (active)steroids in vivo, Epilepsy Behav 127 (2022) 108526.
[82] T. Maurice, Protection by sigma-1 receptor agonists is synergic with donepezil, but not with memantine, in a mouse model of amyloid-induced memory impairments, Behav. Brain Res. 296 (2016) 270–278.
[83] L. Zhao, J.L.-S. Au, M.G. Wientjes, Comparison of methods for evaluating drug-drug interaction, Front. Biosci. 2 (2010) 241–249.
[84] T.-C. Chou, Theoretical Basis, Experimental Design, and Computerized Simulation of Synergism and Antagonism in Drug Combination Studies, Pharmacol. Rev. 58 (2006) 621–681.
[85] T.A. Halgren, Merck molecular force field. I. Basis, form, scope, parameterization, and performance of MMFF94, J. Comput. Chem. 17 (1996) 490–519.
[86] J. Cheung, E.N. Gary, K. Shiomi, T.L. Rosenberry, Structures of Human Acetylcholinesterase Bound to Dihydrotanshinone I and Territrem B Show Peripheral Site Flexibility, ACS Med. Chem. Lett. 4 (2013) 1091–1096.
[87] A. Meden, D. Knez, M. Jukič, X. Brazzolotto, M. Gršič, A. Pišlar, A. Zahirović, J. Kos, F. Nachon, J. Svete, S. Gobec, U. Grošelj, Tryptophan-derived butyrylcholinesterase inhibitors as promising leads against Alzheimer's disease, Chem. Commun. 55 (2019) 3765–3768.
[88] Schrödinger's covalent reactions repository: https://learn.schrodinger.com/private/edu/release/current/Documentation/html/covalent_docking/covalent_docking_user_manual/covdock_reactions_repository.htm (accessed 18 August 2025).
[89] J.L. Banks, H.S. Beard, Y. Cao, A.E. Cho, W. Damm, R. Farid, A.K. Felts, T. A. Halgren, D.T. Mainz, J.R. Maple, R. Murphy, D.M. Philipp, M.P. Repasky, L. Y. Zhang, B.J. Berne, R.A. Friesner, E. Gallicchio, R.M. Levy, Integrated Modeling Program, Applied Chemical Theory (IMPACT), J. Comput. Chem. 26 (2005) 1752–1780.
[90] T. Maurice, B.P. Lockhart, A. Privat, Amnesia induced in mice by centrally administered β-amyloid peptides involves cholinergic dysfunction, Brain Res 706 (1996) 181–193.
[91] V. Lahmy, J. Meunier, S. Malmström, G. Naert, L. Givalois, S.H. Kim, V. Villard, A. Vamvakides, T. Maurice, Blockade of Tau Hyperphosphorylation and Aβ1–42 Generation by the Aminotetrahydrofuran Derivative ANAVEX2-73, a Mixed Muscarinic and σ1 Receptor Agonist, in a Nontransgenic Mouse Model of Alzheimer's Disease, Neuropsychopharmacol 38 (2013) 1706–1723.
[92] B. Li, E.G. Duysen, M. Carlson, O. Lockridge, The Butyrylcholinesterase Knockout Mouse as a Model for Human Butyrylcholinesterase Deficiency, J. Pharmacol. Exp. Ther. 324 (2008) 1146–1154.